Realistic Galaxy Simulations: Feedback, Magnetic Fields and the ISM

Realistic Galaxy Simulations: Feedback, Magnetic Fields and the ISM

By Hector Robinson, B.Sc

A Thesis Submitted to the School of Graduate Studies in the Partial Fulfillment of the Requirements for the Degree Master of Science

McMaster University

McMaster University
Master of Science (2021)
Hamilton, Ontario (Department of Physics and Astronomy)

TITLE: Realistic Galaxy Simulations: Feedback, Magnetic Fields and the ISM
AUTHOR: Hector Robinson (McMaster University)
SUPERVISOR: Dr. James Wadsley
NUMBER OF PAGES: ix, 83

Abstract

The evolution of galaxies rely on a wide variety of physics, and numerical simulations are one of the main tools used to study them. In this thesis we develop a framework for what models can be used to realistically simulate galaxies and study their evolution. We begin with setting specific requirements on the numerical resolution of galaxies, and then test the effects of different stellar feedback models on isolated disk galaxies. We then investigate the addition of magnetic fields into the simulations, and what role they play in determining the contents, behaviour, and star formation, within the interstellar medium of galaxies.

Acknowledgements

I would like to thank my supervisor Prof. James Wadsley for the endless support and guidance he has shown over the last two years. I would also like to thank Prof. Ralph Pudritz and Prof. Alison Sills for their mentoring and support on my committee.

I'd like to send a big shout out to my good friends and colleagues Dennis, Jacqueline, Sachin and Anita, who all worked through this degree with me. I already miss having you guys around. I'd also like to send a big thanks to Joey who's been an amazing mentor/friend/roommate through everything.

Finally I'd like to thank all of my family, especially my Mom, Dad, Grandma and Grandpa, without whose limitless support and "not-frequent-enough" phone calls none of this would have been possible.

Contents

List of Figures

List of Tables

Chapter 1

Introduction

1.1 Galaxies: Introduction

The goal of astronomy and astrophysics is to make sense of what we see in the universe. Of all the things we see, galaxies have proven to be one of the hardest to make sense of. This is because galaxies are nonlinear; the physics that affects galaxies spans many orders of magnitude, in both space and time. The evolution of a galaxy is largely driven by life and death of stars within their interstellar medium, but is also affected by their cosmological location. Stars are about a billion (10^9) meters across, while galaxies and their environments are kiloparsec (10^{19} m) scale objects. Connecting these scales is a difficult task that pieces together techniques from every field of astronomy.

Much of what we know about galaxies comes from many decades of research into stars. In the visible spectrum, almost all of the light from a typical galaxy comes from its stars. Theories of stellar structure predict that the more massive a star is, the bluer its light, and the shorter its lifespan. Conversely, low mass stars are more red, and longer lived. Thus, if a galaxy appears blue, it has plenty of recently formed massive blue stars, indicating that star formation is ongoing. A redder galaxy only contains only the long-lived red stars, meaning that star formation has ceased.

Galaxies have also provided many insights into cosmology. Astronomers quickly realized that while the light we see in galaxies comes from regular baryonic matter, dark matter that interacts only gravitationally must be present galaxies as well. What exactly dark matter is on a particle level remains a mystery, but how it behaves on

astronomical scales has become a precise science. Studies from groups such as the Planck collaboration have measured the fraction of each type of matter to remarkable precision. We now know that dark matter makes up roughly 85% of all the matter in the universe (Planck Collaboration et al. 2018). On the largest scales dark matter is arranged into a cosmic web, with dense halos at intersections of filaments and walls, separated by voids that contain hardly any matter at all. Galaxies sit within the centers of dark matter halos, and thus their behaviours are largely controlled by dark matter.

Another important concept for studying galaxy evolution comes from the finite speed of light. Light emitted from far away galaxies takes time to reach us, which means that the further away we look the longer that light has been travelling and the further back in time the image we see was emitted. This allows us to effectively look back in time and see how galaxies looked throughout the history of the universe. What we see as we look into the Universe is an untold population of galaxies, and by studying this population we can learn how they evolve. Any individual galaxy varies greatly in its properties from the next, but because we can see so many of them, all at different stages of their own evolution, large scale relationships that galaxies tend follow have been found. Theories and simulations of galaxy evolution must operate within the constraints of these relationships and be capable of reproducing them. Theories also go further than reproducing observations; they give us insights into how galaxies work, and inform decisions for future astronomers.

1.2 Galaxies: Current Properties

When viewing the distribution of galaxies, two distinct populations begin to stand out. This is most obvious when plotted on mass-colour diagram (see Figure 1.1). The first population contains low-mass blue galaxies, known as the blue cloud. The second contains higher-mass galaxies that are more red in colour, known as the red sequence (Schawinski et al. 2014). When the shapes of those galaxies are considered, it is seen that the blue cloud is made up of almost entirely 'late-type' galaxies, which are spiral shaped, and the red sequence is made up of 'early-type' elliptical galaxies. The blue colour of spiral galaxies comes from a higher presence of young massive stars,

indicating higher amounts of ongoing star formation. Conversely, red elliptical galaxies tend to have lower star formation rates (see Blanton and Moustakas (2009)). Our own Milky Way Galaxy is thought to be a somewhat typical blue spiral that forms stars at a rate of 2-4 $M_{\odot}$/yr.

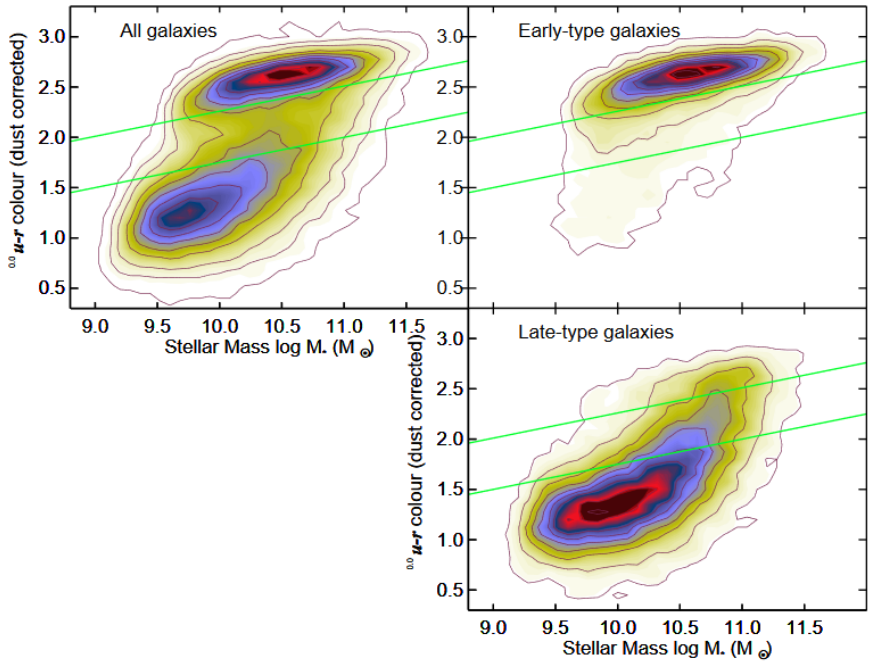

FIGURE 1.1: Colour mass diagram for a population of galaxies. Shown in the top right panel are only early type (elliptical) galaxies. In the bottom right panel only late type (spiral) galaxies are shown. From Schawinski et al. (2014)

Another important component of a galaxy is its supply of gas to form stars with. The xCOLD GASS survey (Saintonge et al. 2017) completed a census of the cold molecular gas content of over 500 galaxies. The authors found that the average molecular gas fraction $f_{H_2} = M_{H_2}/M_{\text{stars}}$ was on average 10% for galaxies with stellar masses of less than 5×10^{10} $M_{\odot}$, but then plummets to 1% as M_{stars} increases to 10^{11} $M_{\odot}$. This drop in cold gas content corresponds to the transition from the blue cloud to the red sequence as seen in Figure 1.1. Blue star forming galaxies have a rich supply of gas fueling star formation, and red passive galaxies are gas poor.

Inside of star forming galaxies, the rate at which a galaxy forms stars is correlated to the surface density of gas. This arises in what is known as the Kennicutt-Schmidt relation (Schmidt 1959; Kennicutt 1998) which relates star formation surface density ($\Sigma_{\rm SFR}$) to gas surface density ($\Sigma_{\rm gas}$):

$$\Sigma_{\rm SFR} = A\Sigma_{\rm gas}^{N} \tag{1.1}$$

Where $N = 1.4$ and $A = 2.5 \times 10^{-4}$. This relation holds for many different types of galaxies such as regular spirals, starbursts, and low surface brightness galaxies. Figure 1.2 shows the global Kennicutt-Schmidt relation. This is not a perfect relationship, there exists some uncertainty, and individual galaxies can vary from the prediction by an order of magnitude.

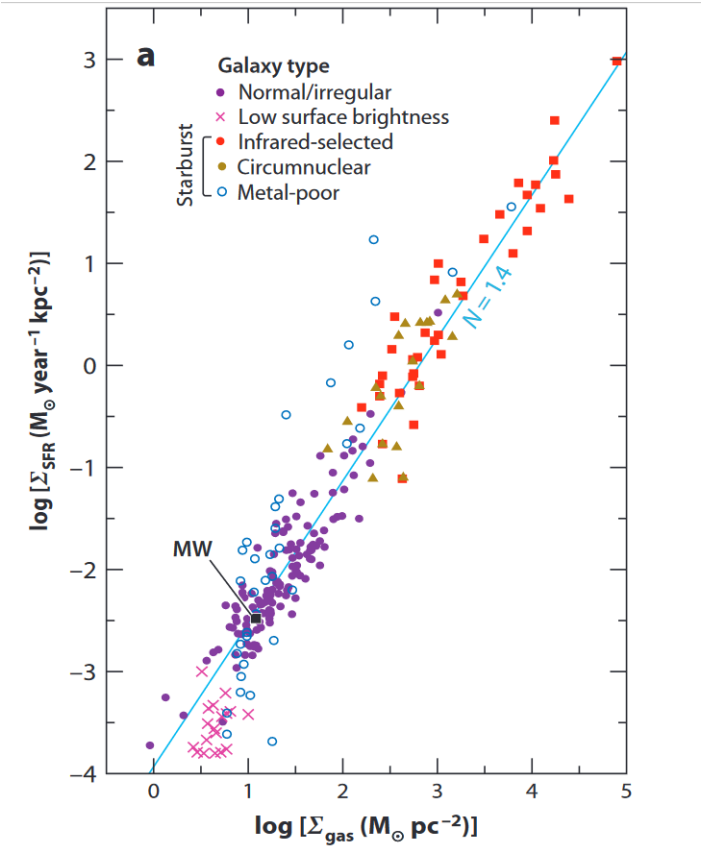

FIGURE 1.2: Global Kennicutt-Schmidt relation. From Kennicutt and Evans (2012)

Combining the previous results paints a basic picture of how galaxies work. Galaxies in the blue cloud have plenty of cold gas and will convert that gas into stars. The red sequence is made up of galaxies that formed stars long ago and have already used up their supply of gas. The remainder of this thesis will concern only blue, spiral, 'Milky Way-like' galaxies. Plenty of questions remain as to how they work. What determines the rate of star formation? What determines how much cold gas is available for star formation? What determines the internal structures within spiral galaxies? The answer to these questions lies in the interstellar medium, where many different types of physics becomes relevant.

1.3 The Interstellar Medium (ISM)

The ISM is the gas and dust that fills the space between stars in a galaxy and provides the fuel for star formation. The ISM is a multi-phase medium with many different temperatures and densities of gas coexisting (see Table 1.1).

The hot ionized medium (HIM) fills most of the volume around a galaxy with diffuse gas of temperatures around 10^6K. How much of the volume within galaxy's disk that is occupied by HIM is not well constrained. This gas is heated from supernovae and stellar winds (McKee and Ostriker 1977), and is likely vented vertically out of the disk before cooling and raining back down onto the galaxy in a fountain-like effect. Hot gas is observed with UV absorption lines and X-ray line emission.

The warm phase of the ISM sits at around 8000 K, containing both neutral and ionized gas. Warm neutral gas is detected via the 21 cm emission line of the hydrogen atoms in the gas, caused by a spin flip of the electron. Warm ionized gas is detected via the Hα recombination line, that has a wavelength of 656 nm. The warm medium is thought to fill a large fraction of the volume within a few hundred parsecs of the galaxy midplane. The cold neutral medium (CNM) exists as clouds of neutral hydrogen at a temperature around 80K, and fills a relatively low volume. Giant molecular clouds (GMCs) are embedded within the clouds of the CNM. GMCs include all gas with densities above 100 cm^{-3}, with temperatures of 10K or less. The gas within GMCs is shielded from radiation which means it can exist in a molecular state. Molecular gas is very difficult to directly observe so tracer molecules are used to infer its presence. The

Phase	T (K)	n (cm^{-3})	Scale Height (pc)
Hot Ionized Medium	10^6	0.003	3000
Warm Ionized Medium	8000	0.1	900
Warm Neutral Medium	8000	0.5	220
Cold Neutral Medium	80	50	94
Giant Molecular Clouds	20	>100	75

TABLE 1.1: Data taken from table 1.1 in Tielens (2005). Summarizes different phases of the ISM.

most common tracer used is carbon monoxide, which has an emission line detectable at a wavelength of 2.6 mm. The cores of GMCs is where star formation occurs, where densities reach up to 10^5 cm^{-3}.

In recent decades, radio interferometry has been used to observe galaxies at resolutions high enough to map the gas within their ISMs. The THINGS survey (Walter et al. 2008) mapped the HI content of 32 nearby galaxies at resolutions of 100-500 pc. THINGS data was used to show that the Kennicutt-Schmidt relation, which was thought to be a global relation for entire galaxies, also held on sub-kpc scales (Bigiel et al. 2008). Recent surveys such as EDGE-CALIFA (Levy et al. 2018) and PHANGS-ALMA (Sun et al. 2018) observed the molecular gas content at even higher resolutions. A quantity that is possible to derive from these observations is called the depletion time, which is defined as the time it would take all of the gas to turn into stars if the current star formation rate continues.

$$t_{dep} = \Sigma_{gas}/\Sigma_{SFR} \tag{1.2}$$

Leroy et al. (2013) measured the depletion time of molecular gas in nearby galaxies averaged over 1 kpc scales and showed the average depletion time is around 1 Gyr. But the measurements of depletion times come with uncertainties of their own. Kruijssen et al. (2018) devised a uncertainty principle for relating the effective beam size of the telescope to the error in the measurements. Measurements centered on peaks in the gas distribution will report artificially higher depletion times and measurements centered on star formation tracers will report lower depletion times.

The observed depletion time measurements are surprisingly long. One might expect clouds to collapse in a freefall and form stars, this would happen on timescales of

$$t_{ff} = \sqrt{3\pi/32G\mu_H n} \tag{1.3}$$

where μ_H is the mean molecular weight of hydrogen, and n is the number density of the gas. This corresponds to timescales of 10 Myrs inside of GMCS, 100 times faster than measurements of depletion times. Actual star formation is also very inefficient, in fact only $\sim 1\%$ of gas within GMCs ends up being converted to stars within a freefall time (Krumholz and Tan 2007). Why star formation is so slow and inefficient may depend on a variety of physics discussed in the following section.

1.4 Physics in the ISM

The ISM is a self-regulating system. There is a constant struggle between gravity compressing gas, and effective pressures in the gas resisting collapse. The different phases of gas are constantly in a state of flux with each other as a result of many different physical processes. Some processes are understood very well, other are less well constrained. A selection of physical processes important to the ISM are summarized here.

1.4.1 Gravity

The gas in a galactic disk is not unaware that it is in a galaxy. The gas is compressed by its own weight, which is set by the gravity of different components of the galaxy. Near the midplane, the gravitational potential comes primarily from the stellar disk, but higher above the disk gravity from the dark matter halo dominates. The weight of the gas sets a pressure at the midplane required to hold the ISM up. The support pressure of the gas is composed of the classical thermal pressure, as well as magnetic fields, cosmic rays, and turbulent motions of the gas.

When a cloud of gas becomes compressed enough, its own internal gravity will become more important than the galactic potential and the cloud will become self-gravitating. This is commonly discussed in terms of a Jeans length (λ_j), which is the

minimum radius a cloud of given density (ρ_0) necessary for collapse.

$$\lambda_j = \sqrt{\frac{15kT}{4\pi G\mu m_H \rho_0}} \tag{1.4}$$

where k is the Boltzmann constant, T is the temperature of the gas, G is the gravitational constant, μ is the mean molecular weight of the gas, m_H is the mass of hydrogen (Carroll and Ostlie 2006). If a cloud is larger than its Jeans Length it will collapse under its own gravity, but if it is smaller the internal energy of the gas will stabilize it against collapse. Several simplifying assumptions go into deriving this version of the Jeans Length, such as assuming the cloud is isothermal, and neglecting the effects of turbulence and magnetic fields. Nevertheless, it provides a rough estimate for when gas will collapse under self gravity. The only variable in Equation 1.4 that isn't constant is the temperature of the cloud, meaning the stability of the cloud depends on primarily on its temperature, which is controlled by heating and cooling processes.

Another common stability parameter is the Toomre Q parameter, given by

$$Q = \frac{c_s \kappa}{\pi G \Sigma_{gas}} \tag{1.5}$$

where c_s is the sounds speed, and κ is the epicyclic frequency (the frequency at which a perturbed piece of gas will oscillate) (Toomre 1964). The Toomre Q parameter describes the stability of an entire disk of gas. For $Q > 1$ the disk is stable against gravitational collapse, and for $Q < 1$ it is unstable. The Toomre Q parameter is appropriate for much larger scales than the Jeans criterion, often used for an entire galactic disk rather than an individual cloud.

1.4.2 Heating & Cooling

Heating and cooling serve to balance the energy of gas in the ISM. Gas that is warm or hot will spontaneously lose energy through radiative cooling, releasing its energy in the form of emitted photons. Line emissions in metal species such as ionized carbon dominate the cooling budget at temperatures beneath 10^4K. At temperatures above 10^4K collisional excitation of neutral hydrogen dominates.

Heating is the second half of the equation. While the gas cools spontaneously, other processes are simultaneously heating the gas. The most effective process is photo-ionization which couples the gas to radiation fields within the galaxy. Stray photons collide with atoms and transfer kinetic energy to their electrons, which then in turn share it with other atoms and electrons in the gas, providing an effective heating. In regions near hot stars there are plenty of energetic photons capable of photo-ionizing hydrogen and this is the main source of heating. In the neutral ISM, Far-UV photons ionize dust and polycylic aromatic hydrocarbon molecules via the photoelectric effect. This is the dominant heating process for all of the neutral ISM (Tielens 2005). Other effects that contribute to heating include cosmic rays, x-rays, and turbulence.

With just cooling and heating balancing each other out, it is possible to derive a stable two-phase model of the ISM with a warm and cold phase existing in pressure balance (Field et al. 1969). The simple two-phase model was challenged in the 1970's when observations revealed a background of x-ray light in the galaxy suggesting the presence of a third phase, the HIM, which was capable of emitting them (Burstein et al. 1977; Jenkins and Meloy 1974).

1.4.3 Turbulence

Turbulence is characterized as chaotic changes in the pressure and velocity of a fluid. The interstellar medium is known to be highly turbulent. One method of observing turbulence is by looking at the distribution of densities within the gas. The measured distribution of gas resembles the Kolmogorov scaling law (Kolmogorov 1941), indicating the presence of turbulence (Larson 1981). On scales too small to be resolved by telescopes, the presence of turbulence can be inferred from the broadening of various spectral lines (Bowen et al. 2008; Goldsmith et al. 2008).

Turbulence was a major component missing from early models of the ISM, which did not account for turbulent motions playing a role in resisting against gravitational collapse. Interstellar gas is almost all supersonic, meaning it will undergo Burger's turbulence (Bec and Khanin 2007). In Burger's turbulence, Kinetic energy is injected on large scales before cascading down to smaller scales where it is eventually dissipated. A constant energy supply is needed to sustain the turbulence while it dissipates from viscosity which transforms it into heat.

In the diffuse ISM, the major source of turbulence is kinetic energy need to sustain turbulence can come from from stellar winds, supernova explosions, hydrodynamic shear and instabilities (McNally et al. 2009). Turbulence in diffuse gas provides an effective pressure which dominates in supporting the vertical structure of a galaxy (Ostriker and Shetty 2011; Kim et al. 2011; Benincasa et al. 2016). On smaller scales, such as within of GMCs, magnetohydrodynamics likely plays an important role in sustaining turbulence (Section 1.4.5).

1.4.4 Stellar Feedback

Throughout their lifetime stars return energy to the ISM through a variety of methods. The added energy can be used to resist gravitational collapse and limit nearby star formation. The result is a negative feedback effect, which leads to the self regulation of the ISM. If more stars are formed, more stellar feedback occurs and quickly shuts star formation down. Early models of a three phase ISM only accounted for supernovae explosions as a form of stellar feedback (McKee and Ostriker 1977), but other many other processes in a young stellar population release energy.

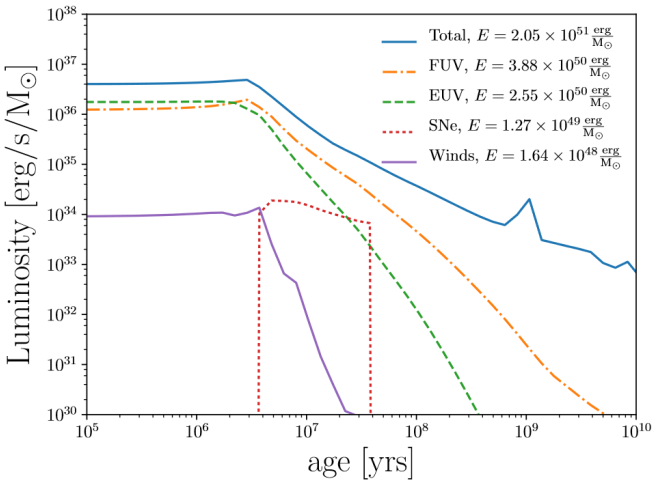

FIGURE 1.3: Luminosity per solar mass as a function of time for a stellar population using the initial mass function (IMF) of Chabrier (2003). The IMF determines how many stars of each mass are initially formed. Chabrier (2003) is a common choice that has a similar functional form to other IMFs used in the field. Taken from Grond et al. (2019).

Figure 1.3 shows the energy released by a stellar population throughout its lifetime. The luminosity of a stellar population is dominated by UV radiation for most of its lifetime. Extreme Ultraviolet (EUV) radiation ($\lambda = 10 - 100nm$) photo-ionizes and heats gas surrounding young stars, creating HII regions, which can transfer momentum into surrounding. Far Ultraviolet radiation ($\lambda = 100 - 300nm$) is not energetic enough to ionize hydrogen, and passes through the surrounding gas, instead heating through the photoelectric effect as described in the previous section (Tielens 2005).

Throughout their lifetime, massive stars will lose mass through stellar winds, ejecting mass and momentum into the surrounding ISM. At the end of their lifetime, massive stars undergo a core collapse type II supernova explosion. On average for every 100 $M_\odot$ of stars formed in a population, one star will undergo a supernova event which deposits $\sim 10^{51}$ ergs of energy into the surrounding gas (Krumholz et al. 2014). The energy of the explosion goes partly into the kinetic energy of swept away surrounding gas, and partly into the thermal energy of the hot bubble created within the expanding cavity. Despite supernova having a low overall luminosity compared to UV radiation, they play a crucial role in stellar feedback, because they inject of momentum which feeds turbulence, and quickly heat gas to temperatures of 10^7 K, where radiative cooling becomes very ineffective (Tielens 2005).

1.4.5 Magnetic Fields

Another important component of a galaxy is magnetic fields. Observations of the Milky Way and nearby galaxies have revealed that magnetic fields are ubiquitous in all spiral galaxies (see Beck and Wielebinski (2013) and references within). The origin of galactic magnetic fields is unknown, but likely small scale 'seed fields' were created in the early universe (Durrer and Neronov 2013) before being amplified by dynamos, which are mechanisms by which the rotational energy of a conducting material is converted into magnetic energy. The small-scale dynamo arises from turbulence in the gas, and can amplify the magnetic field strength to observed values within 10^8 years (Beck et al. 2012; Machida et al. 2013; Rieder and Teyssier 2016). The large-scale dynamo uses the rotation of the galaxy to order the turbulent field into a regular field in about 10^9 years (Ruzmaikin et al. 1988; Beck et al. 1996).

Galactic magnetic fields can be detected through a variety of methods. The only direct measurement is via the Zeeman effect, which is the splitting of spectral lines of atoms in the presence of a magnetic field. Zeeman splitting only measures the component of the magnetic field along the observers line of sight (B_{LOS}), or a lower limit on the total magnetic field (B_{tot}) (eg. Heiles and Crutcher 2005; Crutcher et al. 2010; McBride and Heiles 2013).

Another method of detecting magnetic fields is through the polarization of starlight in the visible and infrared ranges. The polarization is caused by elongated dust grains in the ISM which orient their semi-major axes perpendicular to the magnetic fields (Davis and Greenstein 1951; Hoang and Lazarian 2014). The dust grains extinct different amounts of starlight along semi-major and semi-minor axes, leading to polarization of starlight when particles are oriented along the line of sight.

Relativistic cosmic ray particles emit synchotron radiation when they move through magnetic fields. This synchotron radiation produces diffuse radio emission throughout the Milky Way. Synchotron radiation is linearly polarized, and the position angle of polarization will rotate as the radiation passes through an ionized medium via the Faraday effect. Faraday rotation is sensitive to the direction of the magnetic field, so regular fields will give rise to it while fields with many reversals will not (Beck and Wielebinski 2013).

Zeeman measurements within our own galaxy show magnetic field strengths of 6 ± 2 μG in the cold neutral medium, and inside GMCs field strengths scale with number density $B \propto n^{0.65 \pm 0.05}$ (Crutcher et al. 2010). The Planck satellite constructed all-sky polarization surveys which combined with WMAP data constructed a map of magnetic fields in the Milky Way revealing many loops and filaments implying an highly ordered and regular field (Planck Collaboration et al. 2016). Faraday rotation measurements have revealed large scale reversals in the direction of magnetic fields within the Milky Way (Han et al. 2018). Synchotron measurements of external galaxies show average field strengths of around 10-20 μG (Klein et al. 1991; Fletcher 2010). Starburst galaxies, which have extraordinarily large star formation rates, have fields with strengths of up to 300 μG (Lacki and Beck 2013; Adebahr et al. 2017). External galaxies' fields are also highly ordered, but rarely show field reversals, a puzzling contrast from the Milky way (Beck and Wielebinski 2013).

Magnetic fields also play a role in star formation. Inside of GMCs, magnetic pressure serves as another type of support. If the pressure is enough to support against collapse, the cloud is magnetically subcritical, but if gravity is stronger the cloud is magnetically supercritical. Observations of GMCs have shown that almost all are magnetically supercritical (Crutcher et al. 2010). This implies magnetic fields are not the sole answer to what regulates star formation, but they can still play an important role by resisting turbulent compression and providing pressure support against gravity, although their exact roles in doing this are not yet fully understood (Krumholz and Federrath 2019).

1.5 Galaxy Simulations

One of the main methods for testing models of galaxy evolution is with numerical simulations. Numerical simulations began in the 1970's, at a the time when the available computing power was only enough to study the effects of gravity on a few hundred test particles (Toomre and Toomre 1972). Since then, the power of computers has grown exponentially and modern simulations have grown increasingly complex. Modern galaxy simulations not only solve the equations of gravity, they solve the magnetohydrodynamic equations for interstellar gas, convert gas into stars, model heating/cooling and stellar feedback (see Naab and Ostriker (2017)). That is not to say simulations are no longer limited by computing resources; there is always a compromise to be made between how well you are resolving the physics of the ISM, and with what resources are available to compute them. In even the best galaxy simulations there will always be physics occurring on scales that are too small to be resolved, prompting the use of 'sub grid models' (discussed in Section 2.2) which require extra free parameters that can introduce more uncertainty to the results. Many different approaches to simulate galaxies which resolve different scales have been used by different groups, depending on which physics they are interested in testing.

1.5.1 Cosmological Galaxies

A common approach to simulate galaxies by is simulating a large section of the universe, and letting the galaxies form naturally within the simulation. (Hopkins et al.

2014; Vogelsberger et al. 2014; Schaye et al. 2015; Agertz and Kravtsov 2016; Keller et al. 2016; Grand et al. 2017; Tremmel et al. 2017; Hopkins et al. 2018; Springel et al. 2018). These simulations cover a huge volume and hence have relatively low resolutions. Individual galaxies are not well-resolved but a large population of galaxies is simulated and can be studied. They begin with initial conditions that are based on small fluctuations observed in the Cosmic Microwave Background. They then evolve forward in time inside of an expanding universe. Early cosmological simulations accounted for only dark matter and provided many insights into the large scale structure of the universe, as well as the shapes of dark matter halos. Modern cosmological simulations account for baryonic matter as well, and often focus high resolution on only a single 'zoom-in' region to lower computing time.

Cosmological simulations of galaxies can now fairly reliably predict scaling relations for galaxies, such as the Kennicutt-Schmidt relation, and colour vs. mass relation (Naab and Ostriker 2017). A problem with these types of simulations is that it is complicated to follow the evolution of one individual galaxy. A cosmological galaxy is always changing dramatically due to incoming gas flows, mergers with with other galaxies, star formation bursts, and an ever-changing dark matter halo. Cosmological simulations are also highly chaotic and slight changes in the initial conditions can cause major changes in their properties (Keller et al. 2019). These effects can make it difficult to isolate which physics are most important to galaxy evolution, and some groups choose to simulate individual isolated galaxies instead.

1.5.2 Isolated Galaxies

Moving down a scale, a less common method of galaxy simulations is with individual, isolated spiral galaxies. These can be done at much higher resolution but sacrifice the effects of a galaxies environment. The galaxy will be more well behaved, making it a good place to test out new models of physics, but the lack of a realistic environment means it will not behave entirely realistically over cosmic timescales. For example there will be no incoming gas flows, limiting how long these simulations are useful because eventually the galaxy will run out of gas.

Isolated galaxies are a better arena to test the physics of the ISM because processes such as galactic shear, the formation of individual GMCs, and smaller scale turbulence

become resolvable, however some sub-grid models are still required. These simulations have been used to study the effects of feedback in shaping the ISM (Tasker et al. 2015; Grisdale et al. 2017), the self regulation of the ISM (Benincasa et al. 2016), the evolution of galactic magnetic fields (Dobbs et al. 2016; Rieder and Teyssier 2016; Körtgen et al. 2019), and to compare numerical techniques (Kim et al. 2016).

1.5.3 ISM Boxes

Some groups opt to resolve even smaller scales. Instead of simulating an entire galaxy they simulate a small section inside of a vertically stratified galactic disc. They have periodic boundaries in galactic x-y plane but are open in the vertical z-direction. These simulations can resolve early phases of supernovae feedback, and small-scale structure within clouds, as well as the full lifetime of GMCS (Walch et al. 2015; Kim and Ostriker 2017).

They have been used to show turbulence provides one of the main pressures in a galaxies vertical structure(Ostriker and Shetty 2011). They have also been used to study the effects of feedback and magnetic fields (Walch et al. 2015; Li et al. 2017), and the periodic nature of star formation (Kim and Ostriker 2017).

What these boxes lack is the larger context of the galactic environment. They do not always account for shear or gas inflows, and they have been shown to not be able to corectly model outflows due to their geometry (Martizzi et al. 2016a).

1.6 Thesis Motivation and Overview

The connection between the ISM and galaxy evolution is a difficult problem to simulate. Many groups have tried a wide variety of approaches. In this thesis we explore different approaches and highlight some of the pitfalls. We first begin with some high resolution ISM boxes to calibrate our models before moving to isolated galaxies. The ultimate goal is to simulate realistic galaxies with self-regulating ISMs, while minimizing the use of free parameters to ensure predictive power.

The remainder of this thesis is organized as the following. In Chapter 2 the numerical methods used to conduct our simulations are discussed. In Chapter 3 we present

a suite of small simulations which are used to demonstrate the shortcomings of some methods and explore specific requirements for and limitations on simulating galaxies and the ISM. Once we have chosen a tool-set, we utilize it in Chapter 4 where we add magnetic fields to our simulations and discuss their effects on galaxy evolution. In Chapter 5 our results and future work are discussed.

Chapter 2

Methods

In galaxy simulations, the motions of all the components of a galaxy are calculated numerically. Stars and dark matter are only affected by gravity and can be treated as collections of point particles. The equations of gravity are most often solved with tree-based methods (Barnes and Hut 1986) or particle-particle/particle-mesh methods (Couchman 1991), both of which lower the numerical workload considerably compared to direct calculations. Adding in the dynamics of gas requires accounting for all of the different physics discussed in Section 1.4, which substantially increases the computational expense.

2.1 Hydrodynamics

The motions of the gas are most fundamentally described by hydrodynamics, which is the study of the flow of fluids. The governing equations are called the Euler equations, which can be shown in either a Lagrangian form:

$$\frac{d\rho}{dt} = -\rho \nabla \cdot \vec{v} \tag{2.1}$$

$$\frac{d\vec{v}}{dt} = -\frac{\nabla P}{\rho} + \vec{g} \tag{2.2}$$

$$\frac{du}{dt} = -\frac{P}{\rho} \nabla \cdot \vec{v} \tag{2.3}$$

or Eulerian form:

$$\frac{d\rho}{dt} + \nabla \cdot (\rho \vec{v}) = 0 \tag{2.4}$$

$$\frac{d(\rho\vec{v})}{dt} + \nabla \cdot (\rho\vec{v}\vec{v}) + \nabla P = \rho\vec{g} \tag{2.5}$$

$$\frac{d(\rho u)}{dt} + \nabla \cdot (\rho u + P)\vec{v} = \rho\vec{v} \cdot \vec{g} \tag{2.6}$$

where ρ , $\vec{v}$ and u are the fluid density, velocity and internal energy respectively. P is the thermal pressure and $\vec{g}$ represents body forces such as gravity. The difference between the two forms is only the reference frame. A Lagrangian frame tracks motion from the perspective of an element of the fluid, while the Eulerian frame is a stationary frame that the fluid moves within.

If the effects of magnetic fields are included in the solver, the previous equations are modified into the magnetohydrodynamic equations (shown here in their Eulerian form):

$$\frac{d\rho}{dt} + \nabla \cdot (\rho\vec{v}) = 0 \tag{2.7}$$

$$\frac{d(\rho\vec{v})}{dt} + \nabla \cdot (\rho\vec{v} \cdot \vec{v} - \vec{B} \cdot \vec{B} + P^*) + \nabla P = 0 \tag{2.8}$$

$$\frac{dE}{dt} + \nabla \cdot [(E + P^*)\vec{v} - \vec{B}(\vec{B} \cdot \vec{v})] = 0 \tag{2.9}$$

$$\frac{\partial B}{\partial t} - \nabla \times (\vec{v} \times \vec{B}) = 0 \tag{2.10}$$

where P^* is a diagonal tensor with the component $P^* = P + B^2/2$, and E is the total energy density

$$E = \frac{P}{\gamma - 1} + \frac{1}{2}\rho v^2 + \frac{B^2}{2} \tag{2.11}$$

where $\gamma = 5/3$ is the adiabatic index. Hydrodynamics/magnetohydrodynamics solvers naturally fall under two main categories, Eulerian (grid codes) and Lagrangian (particle or mesh codes).

Eulerian methods discretize space into fixed grids. Fluid is typically transported by calculating fluxes through adjacent grid cells using a Riemann solver (Godunov 1959). To achieve high resolutions grid codes often use Adaptive Mesh Refinement (AMR) to split grid cells into smaller constituents in regions of interest. Eulerian solvers tend to be high order, have low noise, and can resolve shocks well. Their downside comes from

artificial diffusion, poorly computing circular orbits, and computational limits to their timesteps. Some popular Eulerian solvers used in astrophysics are RAMSES (Teyssier 2002), ENZO (Bryan et al. 2014), FLASH (Fryxell et al. 2000), and ATHENA (Stone et al. 2008).

Lagrangian methods discretize mass rather than space. The most common of these methods is known as Smoothed Particle Hydrodynamics (SPH), which splits gas into particles that are free to move and not bound to a grid. Fluid quantities are calculated by a weighted sum over neighbouring particles. For a fluid quantity f_j the SPH smoothed estimate is given by

$$f(\vec{r}) = \sum_{j}^{N} m_j \frac{f_j}{\rho_j} W(\vec{r} - \vec{r_j}, h). \tag{2.12}$$

where N is the number of neighbours summed over. $W(\vec{r} - \vec{r_j}, h)$ is an SPH kernel function, many different functions can be used but it must be spherically symmetric, positively valued, and normalize to 1

$$\int W(\vec{r} - \vec{r_j}, h) d\vec{r} = 1 \tag{2.13}$$

The parameter h is per-particle smoothing length, which sets the width of the kernel function on each corresponding particle. The smoothing length is often set so that N particles are within the domain of $W(\vec{r} - \vec{r_j}, h)$. The pressure force on a particle can then be calculated by using equation 2.12 to solve to density

$$\frac{d\vec{v_i}}{dt} = -\sum_{j}^{N} m_j \left(\frac{P_i + P_j}{\rho_i \rho_j} \right) \nabla_i W_{ij}(h_i) + \vec{g} \tag{2.14}$$

The particle nature of SPH has both benefits and drawbacks. It couples easily with tree-based methods for calculating gravity, and intrinsically conserves mass, energy, and momentum. However it also prevents the mixing of any fluid quantities at sub-resolution scales, which can suppress the growth of fluid instabilities (Agertz et al. 2007). Modern SPH codes correct for this by including geometric density average forces and turbulent diffusion (see Wadsley et al. 2017). Well known SPH solvers in astrophysics include HYDRA (Couchman et al. 1995), GADGET (Springel 2005),

Gasoline (Wadsley et al. 2004; Wadsley et al. 2017), and Phantom (Price et al. 2018).

In addition to particle and grid codes there exist some hybrid methods such as Gizmo (Hopkins 2015), and Arepo (Springel 2010). Arepo discretizes gas onto a Voronoi tessellation rather than a grid and and uses a Riemann solver to compute flux at interfaces. Gizmo is similar to SPH but has higher order momentum exchange estimators. The hybrid models perform as well or better than other methods on some problems. In particular, they handle low speeds and subsonic turbulence better.

Comparison projects have been completed that compare many different codes of each technique to determine if either type is best suited for galaxy simulations (Scannapieco et al. 2012; Kim et al. 2014; Kim et al. 2016). Most conclude that while small differences exist between each technique, there is no clear method that is best. The code used different groups comes down to which is better at the specific problem they are trying to solve.

2.2 Sub-grid Physics

Star formation and stellar feedback cannot practically be resolved in galaxy-scale simulations, because they occur on scales much smaller than even the smallest resolution elements. They must be added in with 'sub-grid' models, which are not derived from first principles like the hydrodynamics. However, free parameters in these models can be calibrated with theories and observations to produce realistic effects. Designing sub-grid models is a balance between tuning them to produce the desired effect on the simulation while not reducing their predictive power. For example a star formation model should be able to predict a realistic star formation rate for a galaxy, without it being hard-coded in to always get the correct answer. A feedback model should heat the ISM and regulate star formation. These two models play hand-in-hand with each other and are usually designed together for a specific code.

The Aquila Comparison Project (Scannapieco et al. 2012) tested the state of galaxy simulations in the field. They simulated galaxies with the same initial conditions using many different codes, and showed that the use of various sub-grid models used led to

a wide variety of predictions for the galaxy's mass, size, gas content, and morphology. Additionally, all codes failed to make predictions consistent with theoretical expectations. Since then there has been a push to develop physically motivated sub-grid models that are based on first principles.

Star formation sub-grid models often begin by using criteria to determine which gas elements (particles or grid cells) are star-forming (Stinson et al. 2006). Some common choices include (1) the gas must be above a threshold density, (2) the gas must be in a converging flow, and (3) the gas must be unstable to Jean's collapse (see Section 1.4.1). If a gas element meets all the criteria, it is allowed to form stars, commonly by a Schmidt-like law, of the form

$$\frac{d\rho_*}{dt} = \frac{\epsilon_* \rho_{gas}}{t_{ff}} \tag{2.15}$$

where ρ_* is the stellar density, and ϵ_* is an efficiency parameter. The left hand side of this equation is the rate at which gas is converted into stars. Because t_{ff} depends on density there is a non-linear dependence dense gas will rapidly be consumed. In the hydrodynamics solver, mass is removed from a star-forming gas element, and a new star particle is created with that mass and with the same position and velocity. Star particles often have much more mass than individual stars, meaning they represent a stellar populations rather than a single star. The ϵ_* parameter is a number between 0 and 1 that limits the efficiency of star formation. By lowering it the star formation can be artificially brought down to levels that match observations. As we will come to see in the following chapters, a lot of important physics can be hidden behind ϵ_*. In the real world, star formation is limited by physical processes, but simulations are not capable of resolving all of them. If effective stellar feedback is used and turbulence in the gas is resolved ϵ_* would not need to be artificially lowered to limit star formation.

Stellar feedback works by returning energy to the ISM from young stars. The simplest method would be to dump 10^{51} ergs of thermal energy for every supernova into the nearest gas element when a star particle undergoes feedback (around 5-10 Myrs after its creation). In practice this method is not very effective because all a supernova's thermal energy is spread out among the whole gas element, rather than localized in an tiny supernova remnant. This results in a lot of gas being heated to warm temperatures rather than a small amount of gas being heated to extreme

temperatures. At warm temperatures the cooling times are still short and all of the supernova's thermal energy will radiates away before having any effect. To address this problem feedback models often prevent gas elements that receive energy from feedback event from cooling (Stinson et al. 2006; Agertz et al. 2011). The amount of hot gas produced by these methods can still be resolution dependent. Keller et al. 2014 developed a 'superbubble' feedback model that accounts for thermal conduction and evaporation between gas phases. The superbubble model is resolution independent introduces minimal free parameters.

An additional sub-grid model used in simulations is a Jean's pressure floor. The pressure floor is a minimum pressure allowed in the gas as a function of density, that stops the gas from unphysically collapsing and fragmenting (Truelove et al. 1997; Robertson and Kravtsov 2008). This is done by enforcing that the local Jeans length is resolved by a minimum number of gas elements. In this work the pressure floor is of the form

$$P_{min} = \frac{1}{\gamma\pi} N_j^2 G \rho_{gas}^2 \Delta x^2 \tag{2.16}$$

where γ is the adiabatic index of the gas (5/3), N_j is the number of elements that the Jeans length is required to be resolved by, and Δx is the size of the resolution elements. While the Jeans floor is in common usage, it is not well characterized how realistic the support it provides is compared to a theoretical "infinite resolution" simulation that would not need it.

2.3 Code Used in this Thesis

In this work we conduct galaxy simulations using a combination of grid codes and SPH. The majority of simulations in Chapter 3 are conducted using the SPH code GASOLINE2 (Wadsley et al. 2017). GASOLINE2 is a modern update of the SPH code GASOLINE (Wadsley et al. 2004), originally built from the gravity solver PKDGRAV (Stadel 2001).

Simulations in Chapter 4 study the effects of magnetohydrodynamics. For that we use the octree-based AMR code RAMSES (Teyssier 2002). RAMSES uses a HLLC Riemann solver (Toro et al. 1994) for regular hydro simulations, and a HLLD Riemann solver (Miyoshi and Kusano 2005) for MHD simulations. RAMSES incorporates the pressure floor with a non-thermal pressure support term given by the temperature polytrope $T_{min} = \mu T_j n_H / n_J$ where μ is the mean molecular weight, and the values of T_j and n_J are adjusted to give the same minimum pressure as in Equation 2.16.

In both GASOLINE and RAMSES, we choose to utilize gas cooling and heating with the equilibrium cooling code GRACKLE (Bryan et al. 2014; Smith et al. 2016). GRACKLE uses tabulated cooling rates from the photo-ionization code CLOUDY (Ferland et al. 2013). The metal cooling rates are given for solar abundances, and are then scaled linearly with the metallicity in the simulation. We use photoelectric heating in GRACKLE, with a heating rate of $\zeta = 4 \times 10^{-26}$ erg cm^{-3} s^{-1}.

2.4 Initial Conditions

Here we describe the processes used to generate the different initial conditions (ICs) used in this thesis:

2.4.1 Periodic ISM boxes

Simulations of ISM boxes are done with GASOLINE. To create an initial uniform gas distribution, the SPH particles are arranged in a glass-like arrangement, as opposed to a grid because this is the natural state they will evolve to with no external forces. We start with an arrangement of particles pre-relaxed into a glass and stretch it to reach to required density. Boundary conditions are periodic in the x and y directions, but open in the z direction. The density of gas is set to be a typical value for the solar neighbourhood in the Milky Way (10 $M_\odot$/pc^2). The temperature of particles is initialized to 10^4 K.

In the ISM boxes that include the effects of gravity, we add an external galactic gravitational force of the form

$$g_z = \frac{z v_c^2}{(R^2 + z^2)} + 2\pi G \Sigma_{gas} \tanh\left(\frac{z}{H_{gas}}\right) \tag{2.17}$$

Where $R = 6$ kpc is the distance to the center of the galaxy, $v_c = 220$ km/s is the circular velocity of the galaxy at radius R, $\Sigma_{gas} = 10\ M_\odot/\mathrm{pc}^2$ is the surface density of gas, and $H_{gas} = 130$ pc is the scale height of the gas disk. We also use the GASPATCH method (Fung 2012) to account for gravity from the far field that is not included in the periodic boundary conditions.

2.4.2 Agora Disk

To model isolated galaxies we use the isolated galaxy disk model from the Agora Comparison Project (Kim et al. 2016). Part of the appeal of this IC is that it is a standard and openly available for many codes. This galaxy IC is meant to emulate a Milky Way like galaxy at redshift ~ 1. The Agora disk contains the following components:

- A dark matter halo with $M_{200} = 1.074 \times 10^{12} M_\odot$, $R_{200} = 205.5$ kpc, and circular velocity of $v_{200} = 150$ km s^{-1}. The halo follows the NFW density profile (Navarro et al. 1997) with concentration parameter $c = 10$ and spin parameter $\lambda = 0.04$. The halo is made of dark matter particles of mass $m_{DM} = 1.25 \times 10^7 M_\odot$ in both Gasoline and Ramses.

- An exponential disk with mass $M_d = 4.297 \times 10^{10} M_\odot$, scale length $r_d = 3.432$kpc, and scale height $z_d = 0.1 r_d$. The disk is 80% stars and 20% gas by mass. In RAMSES, the gas disk is constructed on a grid, and follows and analytic density profile of

  $$\rho_{d,gas}(r, z) = \rho_0 e^{-r/r_d} \cdot e^{-|z|/z_d} \tag{2.18}$$

  with $\rho_0 = M_{d,gas}/(4\pi r_d^2 z_d)$, while in GASOLINE the disk is constructed out of SPH particles.

- A stellar bulge with mass $M_b = 4.297 \times 10^9 M_\odot$. The bulge follows a Hernquist profile (Hernquist 1990), with $M_b/M_d = 0.1$. Stars are represented by particles in both Gasoline and Ramses, however stars included in the IC represent an older stellar population and do not contribute to feedback. Initial star particles have a mass of $m_{star} = 3.4 \times 10^5 M_\odot$
- In the simulations that include MHD, we have added an initial magnetic field to the Agora disk. We intialize the field to be purely toroidal, similar to Körtgen et al. 2019. The field strength scales with the gas density, such that $B \propto \rho^{2/3}$.

Chapter 3

How to Simulate a Galaxy

The goal of this chapter is to develop a set of tools that can be used to simulate galaxies and test the physics in their ISM. We do this by conducting a suite of several different simulations of different scales using a variety of the methods described in Chapter 2. We strive to conduct simulations with predictive power, meaning the models we decide upon must be able to accurately predict the behaviour of galaxies in the regimes of interest. The correct properties and behaviour of galaxies should fall out of the models naturally, without being forced to always give the correct answer. To that end the simulations in this chapter are intended to explore specific requirements and limitations on simulating galaxies and the ISM.

3.1 Periodic ISM box

We first present results from a periodic ISM box simulated using the methods described in Section 2.4.1. The simulation domain is a box with side lengths of 2 kpc that contains $4 \times 10^7 M_\odot$ of gas, giving a surface density of $\Sigma_{gas} = 10 M_\odot / pc^2$, a typical value for the solar neighbourhood in the Milky Way. The box is relaxed for 2 Gyrs under the effects of the galactic potential and radiative cooling to reach an initial steady state with no vertical oscillations left from the IC. The effects of self gravity, star formation, and stellar feedback are left off. After this period the gas settles into a characteristic density profile along the z-axis with a scale height of 39 pc. To test the resolution dependence of this model we run the same thing the gas at a variety of resolutions. The lowest resolution run contains 465 gas particles with a mass of 85900

$M_\odot$. Each subsequent run has twice as many particles, with the highest resolution containing 29773 particles of 1342 $M_\odot$.

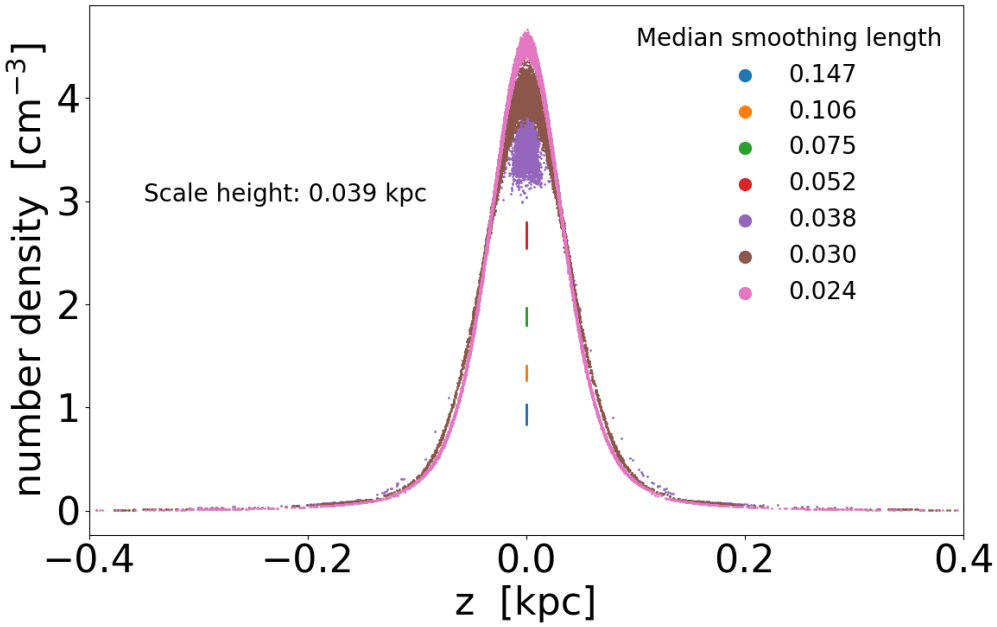

FIGURE 3.1: Density profile of simulated box at multiple resolutions. One point is plotted for every gas particle in the simulation. Different resolution simulations are shown in different colours. The red, green, blue, and orange simulations have collapsed into a 2-dimensional sheet.

The density profile formed for each resolution can be seen in Figure 3.1. At the higher resolutions the result is converged and all simulations form a Gaussian density profile. At lower resolutions the gas fails to resolve the vertical distribution of the gas, and instead the particles collapse into a two-dimensional sheet, any information along the third dimension is lost. This reflects the finite resolution of the hydrodynamical scheme incorrectly interacting with the infinite resolution of the gravitational potential. This is not reflective of any real behaviour of gas under the effects of gravity. There is not a smooth transition to this failure occurring, instead it happens suddenly at resolutions where the median smoothing length of the particles is smaller than the scale height of the disk. Because most of the particles are located in the mid-plane of the disk, the median particle smoothing length represents the size of the average

particle in the mid-plane. What this shows is that in order to resolve a galactic disk, the size of the resolution elements must be no larger than the scale height of the disk. This is a minimum requirement on resolution to simulate a galaxy that has sensible results. Our test was done only in SPH, but this problem has been known to exist in grid codes as well (R. Teyssier, private communications).

The resolutions used in this simulation may appear quite low. In fact it would be easy to substantially increase the resolution on an average computer and still run fairly quickly, so this failure may seem to not pose a real threat to modern simulations. However the simulations presented are only a small piece of an entire galaxy. Simulations of full galactic disks often have resolutions similar to those used here, and under resolving the scale height is a real possibility. For example, the Agora high resolution isolated galaxy (Kim et al. 2016) has a spatial resolution of 80 pc and a scale height of ∼150 pc in the central region, resolving the scale height with 1-2 elements at most. Hence, care must be taken to ensure that the scale height is always resolved.

3.2 Adding Star Formation & Feedback

To test the full capabilities of ISM box we run a new simulation with the same density of gas but with side lengths of 0.5 kpc and a total of 262144 gas particles, giving a mass resolution of 9.375 $M_{\odot}$ or a median smoothing length of 3.7 pc. After being relaxed, the effects of self gravity, star formation and stellar feedback are included. The stellar feedback prescription used is the self-consistent superbubble model (Keller et al. 2014). Figure 3.2 shows a density projection along the y-axis of the simulation at several different times. Because of the addition of self-gravity, the gas disk quickly compresses itself to a scale height that oscillates between 3-12 pc. The first feedback event can be seen occurring around 91 Myr in the second panel of Figure 3.2. After this the simulation becomes quite violent, and multiple feedback events disturb the disk substantially. By the end of the run, roughly a fifth of the total gas mass has been converted into stars and any structure of the original disk is gone.

The time evolution of the gas scale height and star formation rate can be seen in Figure 3.3. The star formation occurs in bursts, which blast gas up out of the midplane. After the star formation burst, the gas falls back down and bounces, oscillating with

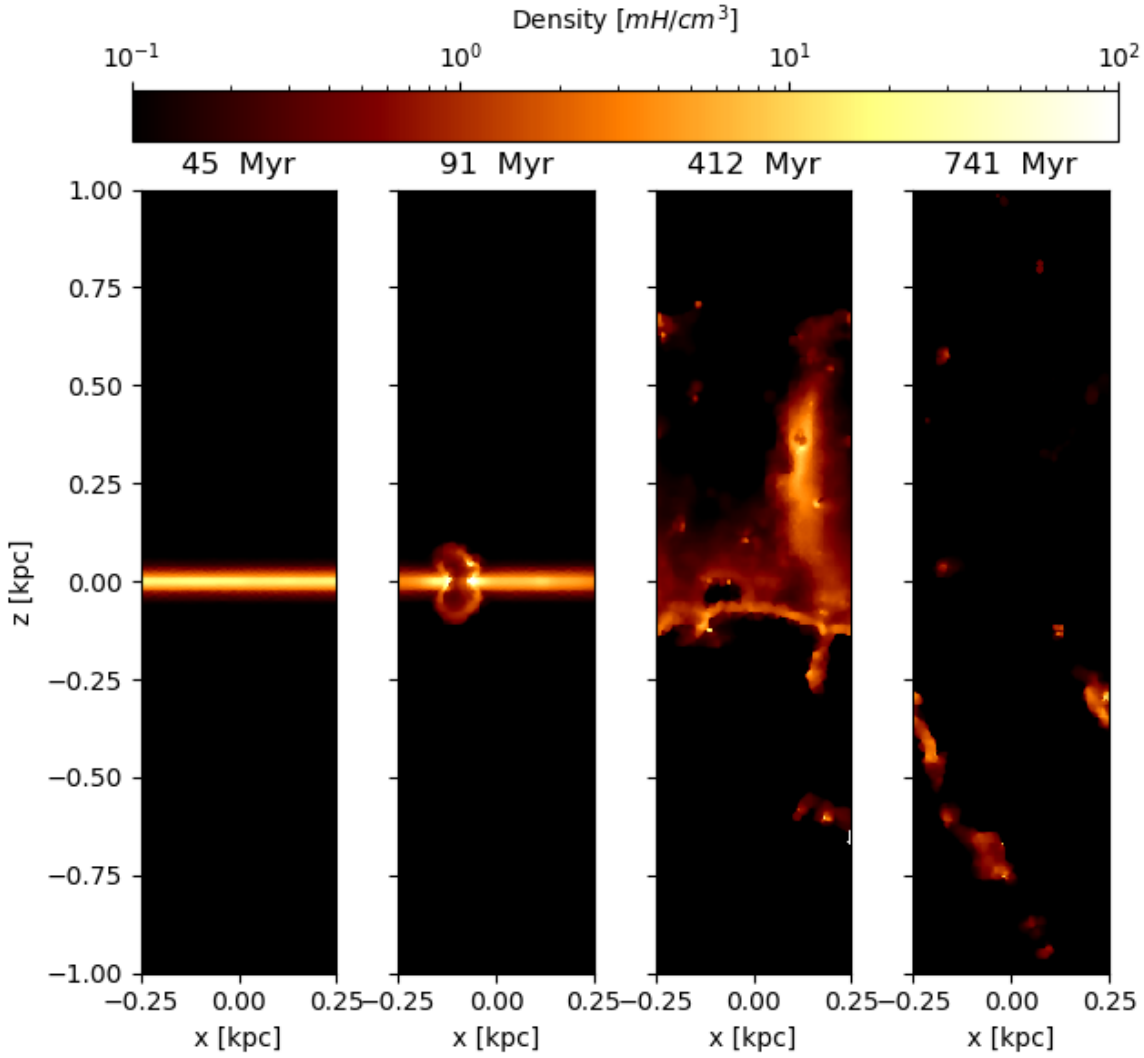

FIGURE 3.2: Time evolution of box simulated with superbubble feedback. Each panel shows a projection of the gas density along the y-axis.

a period of ∼90 Myr. After a few oscillations the gas is relaxed and compressed in the midplane again, and another star formation burst takes place. Each subsequent burst is smaller than the previous. This periodic behaviour makes it difficult to study the structure of the interstellar medium. The gas scale heights are of order kiloparsecs, much larger than expected values of tens or hundreds of parsecs in disk galaxies, and the vertical motions of the gas suggest velocities of ∼1000 km/s, much larger than any seen in nearby galaxies.

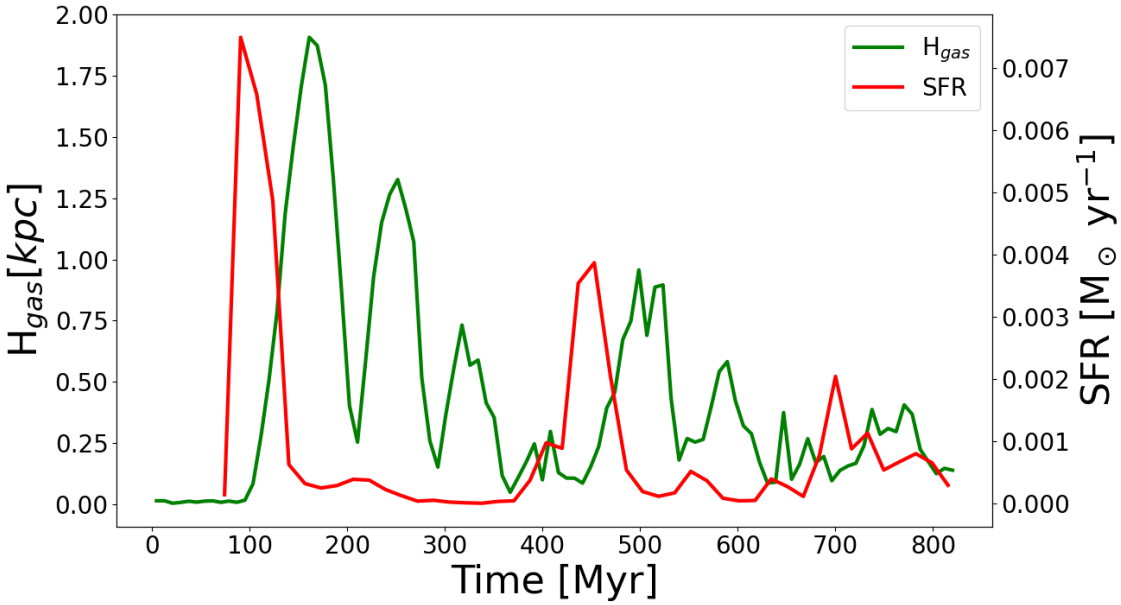

FIGURE 3.3: Time evolution of gas scale height and surface density of periodic box with superbubble feedback over time.

Altogether these results suggest the periodic ISM box is perhaps not the best place to study the self regulating effects of star formation, feedback and turbulence in the ISM. As discussed in Martizzi et al. (2016a) this arises from the fact that the cartesian box does not capture the correct global geometry of potential of a real galaxy. Effects such as galactic shear and any internal structure of the galaxy are ignored. Additionally, the superbubbles formed from the feedback grow larger than the size of the box. In a real galaxy they would have space to expand along the x and y axis before falling back down onto the galaxy, but the bubbles are effectively trapped in a tunnel that funnels them straight up and down. For all these reasons we choose to study entire disk galaxy simulations for the remainder of this thesis.

3.3 Isolated Galaxy

Our first entire galaxy simulation uses the Agora isolated disk galaxy, with an identical setup to that used in the GASOLINE run from the Agora Comparison Project (Kim et al. 2016). Feedback is handled through a simple thermal energy dump of 10^{51} ergs for

every 91 $M_\odot$ of stars formed, also ejecting 14.8 $M_\odot$ of gas including 2.63 $M_\odot$ of metals. Star formation occurs in any gas above a threshold density of $\rho_{star} = 10\ m_p/cm^{-3}$ with an efficiency parameter $\epsilon_* = 0.01$, and a pressure floor is included. The galaxy sits at the center of a simulation domain that is a cube with side length of 600 kpc. The gas particles have a mass resolution of 8.5 $\times 10^4$ $M_\odot$, or an average size of 73.2 pc.

A detailed analysis of many of this galaxy's properties are available in Kim et al. 2016, but we shall restrict our analysis to the effects of the stellar feedback on the morphology and star formation history of the galaxy. To do this we run a second galaxy using identical settings, except that no stellar feedback is included. Comparing the runs with and without feedback is used to determine the behaviour of the feedback model.

Figure 3.4 shows the evolution of both galaxies face-on. They both start off as an initial smooth disk which can be seen in the top panel. In the middle panel (164 Myrs), spiral arm features have begun to develop and many variations in the gas density can be seen. The final snapshot (536.8 Myrs) is shown in the bottom panel, by this time the gas is much more clumped, and the spiral arms are fully developed. Minor differences in the structure of the arms can be seen between the galaxy with and without feedback but there is no major differences between their overall structure. Figure 3.5 shows the same snapshots but now faced edge-on to the galactic disk. Again there is no major differences between the galaxies. Neither galaxy has any vertical outflows of gas, despite that being an expected result for the galaxy with stellar feedback. The use of stellar feedback apparently did not play an important role in shaping the morphology of this galaxy.

The star formation history of both galaxies is shown in Figure 3.6. Both galaxies have a SFR (star-formation rate) that steadily increases to 2.5 $M_\odot$/yr. What is notable is that both galaxies have essentially the same SFR throughout their entire histories. Another way of looking at star formation is through the Kennicutt-Schmidt relation, which is shown in Figure 3.7, which shows the density of gas that stars are forming in. Both galaxies match the observed relation from Kennicutt et al. 2007 quite well. Despite one galaxy including stellar feedback and the other having none, the star formation occurs almost identically in both.

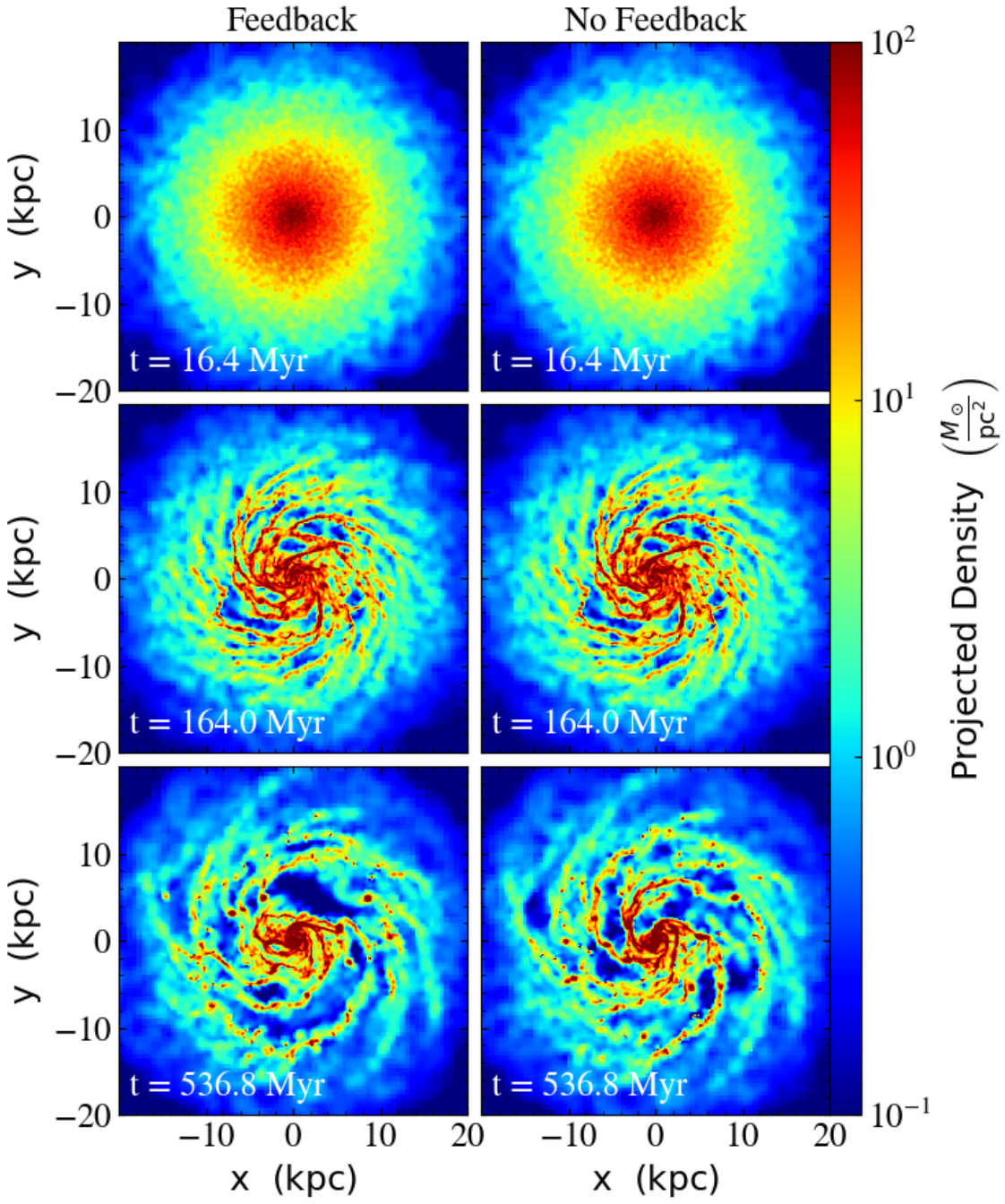

FIGURE 3.4: Time evolution of simulated galaxies with and without stellar feedback (left and right columns respectively). Each panel shows a projection of the gas density along the z-axis.

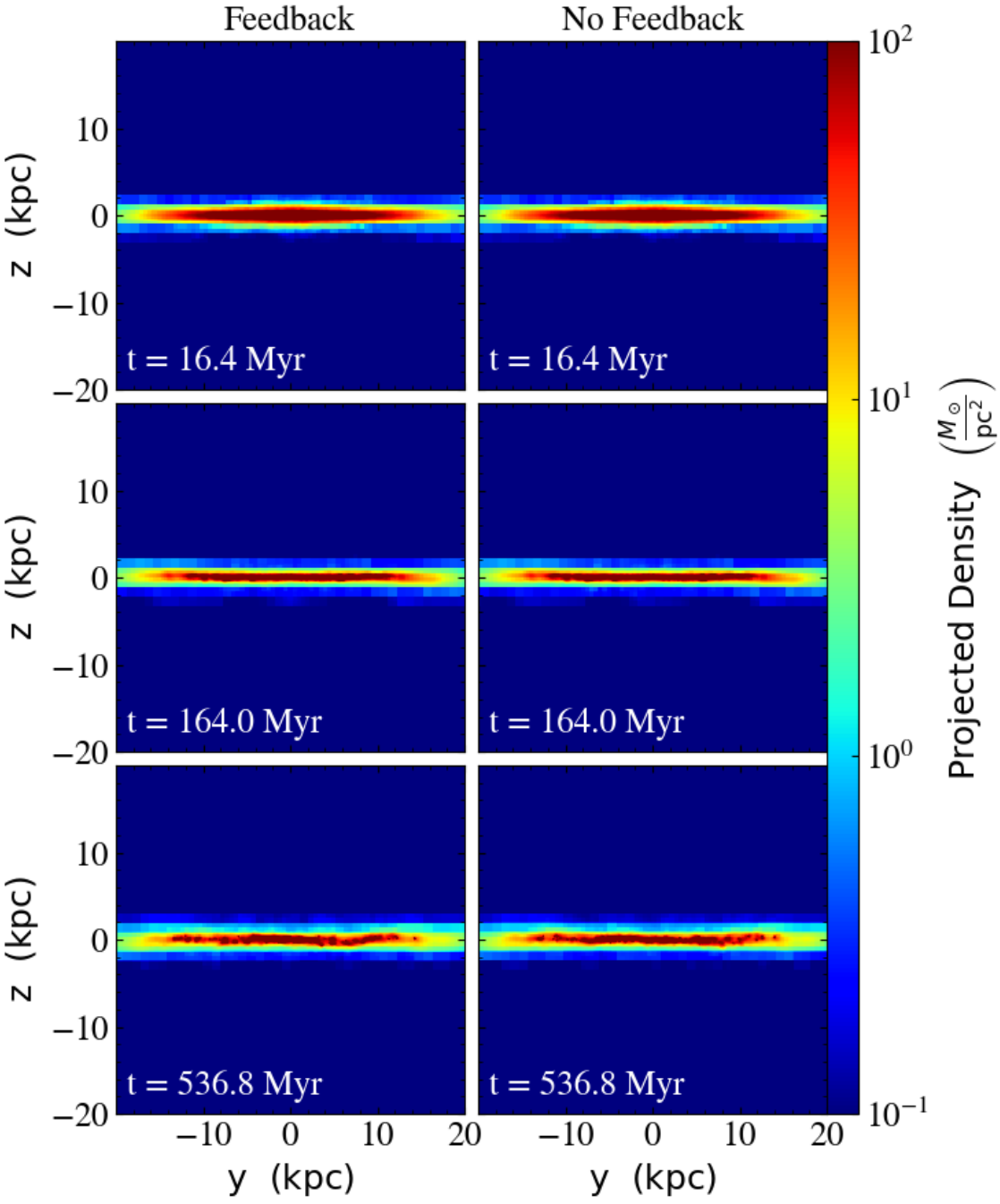

FIGURE 3.5: Time evolution of simulated galaxies with and without stellar feedback (left and right columns respectively). Each panel shows a projection of the gas density along the x-axis.

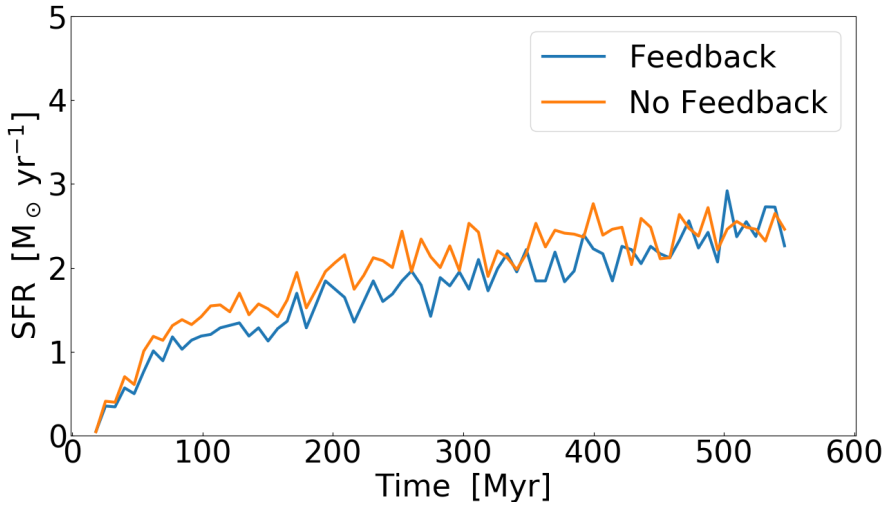

FIGURE 3.6: Star formation history of simulated galaxies with and without stellar feedback

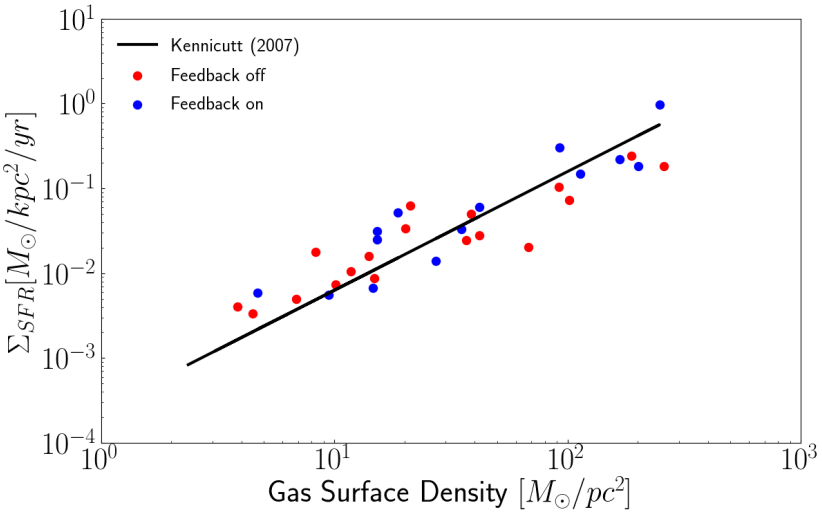

FIGURE 3.7: Kennicutt-Schmidt relation for simulated galaxies with and without stellar feedback.

Neither the star formation or morphology of the galaxy is affected by the use of stellar feedback. In fact for all intents and purposes both galaxies appear to be identical. This is a problematic result because feedback models were originally implemented to regulate star formation. The feedback model has failed to create any meaningful

changes to the evolution of this galaxy. In the place of self-consistent regulation of the ISM, star formation is only being limited artificially by the use of the efficiency parameter $\epsilon_* = 0.01$. This is essentially cheating to ensure the Kennicutt-Schmidt relation holds. But if we want instead to rely on stellar feedback to regulate star formation, we must first answer why the feedback model failed.

3.4 Why did the Feedback Fail?

To test the feedback model we conduct a test simulation that consists of a single star particle in a periodic box of gas. The box is periodic in all three dimension, and this should represent a supernova event occurring within the cold phase of the ISM. The box has side lengths of 2.5 kpc and a density of 10 m_p/cm^{-3}. The star particle has a mass of 10^6 $M_\odot$. After 1 Myr it undergoes feedback using an identical setup to the isolated galaxy. We run the identical simulation with three different resolutions. The lowest resolution has gas particles with a mass of 10^5 $M_\odot$, the same resolution as the isolated galaxy run. The increased resolutions have 8 times as many gas particles with 1/8th the mass, and 64 times as many gas particles with 1/64th the mass.

Each feedback event adds energy to the gas particles with a thermal energy dump into the nearest particles. A temperature slice of the bubble of hot gas that is created can be seen in the left column of Figure 3.8. In the low resolution case, the bubble appears as a perfect circle, because all of the hot gas is a single gas particle. The increased resolution cases have more complicated structures, and resolve a shell of warm gas surrounding the hot interior of the bubble. The energy added to the box is plotted versus time in the right hand column. In all three cases, some of the thermal energy is converted in kinetic energy as the bubble expands. The lowest resolution case has the least kinetic energy at all times, but interestingly the medium resolution case has more kinetic energy than the high resolution case, pointing to the results still not being converged. While some thermal energy is converted into kinetic, more of it is lost through radiative cooling. This happens most dramatically in the low resolution case where all of the thermal energy (and hot gas) is gone in less than 1 Myr. As the resolution is increased, the thermal energy radiates away slower. This is because

in the higher resolution cases less gas is heated, so the temperatures go higher where there is lower cooling rates.

This demonstrates that the feedback model failed to limit star formation in the isolated galaxy because the resolution used was too low. At high resolutions hot gas stay around for longer which would in turn limit gravitational collapse. The low resolution case used in this simulation was the same resolution used in the isolated galaxy simulation. The feedback failed to affect the galaxy in any meaningful way because the energy artificially cooled away before it could have any affect. There does not appear to be a specific resolution where it begins to work like in the case of resolving the scale height in section 2.4.1. Instead it seems the feedback model continuously improves as the resolution is increased. Simply increasing the resolution of the isolated galaxy is not a solution because we rapidly approach resolutions not feasible in entire galaxy simulations. The solution then is to use an entirely new feedback model that is resolution independent.

3.5 Delayed Cooling Feedback

The goal is now to choose a feedback model that can be used in our isolated galaxy to correct predict the behaviour of the ISM, without relying on an unrealistically low star formation efficiency. In the previous section we determined that a simple thermal energy dump will not work, so we now move to the slightly more complicated delayed cooling feedback method described in Agertz et al. (2011). This method prevents gas that has received energy from a supernova event from cooling for 5 Myr. This allows the supernova remnant to adiabatically expand before the energy all radiates away due to low numerical resolutions. Our following simulations are done using the RAMSES AMR code which has delayed cooling feedback implemented. RAMSES was used in the original Agora simulations and had no major differences from the GASOLINE run. The failure of the simple feedback model occurs in both codes. Additionally, we set the star formation efficiency parameter to $\epsilon_* = 0.1$, as opposed to 0.01 in the previous section. This is a much more realistic value for the efficiency, but if left unchecked star formation will occur at incredible rates, unless the new feedback model is working.

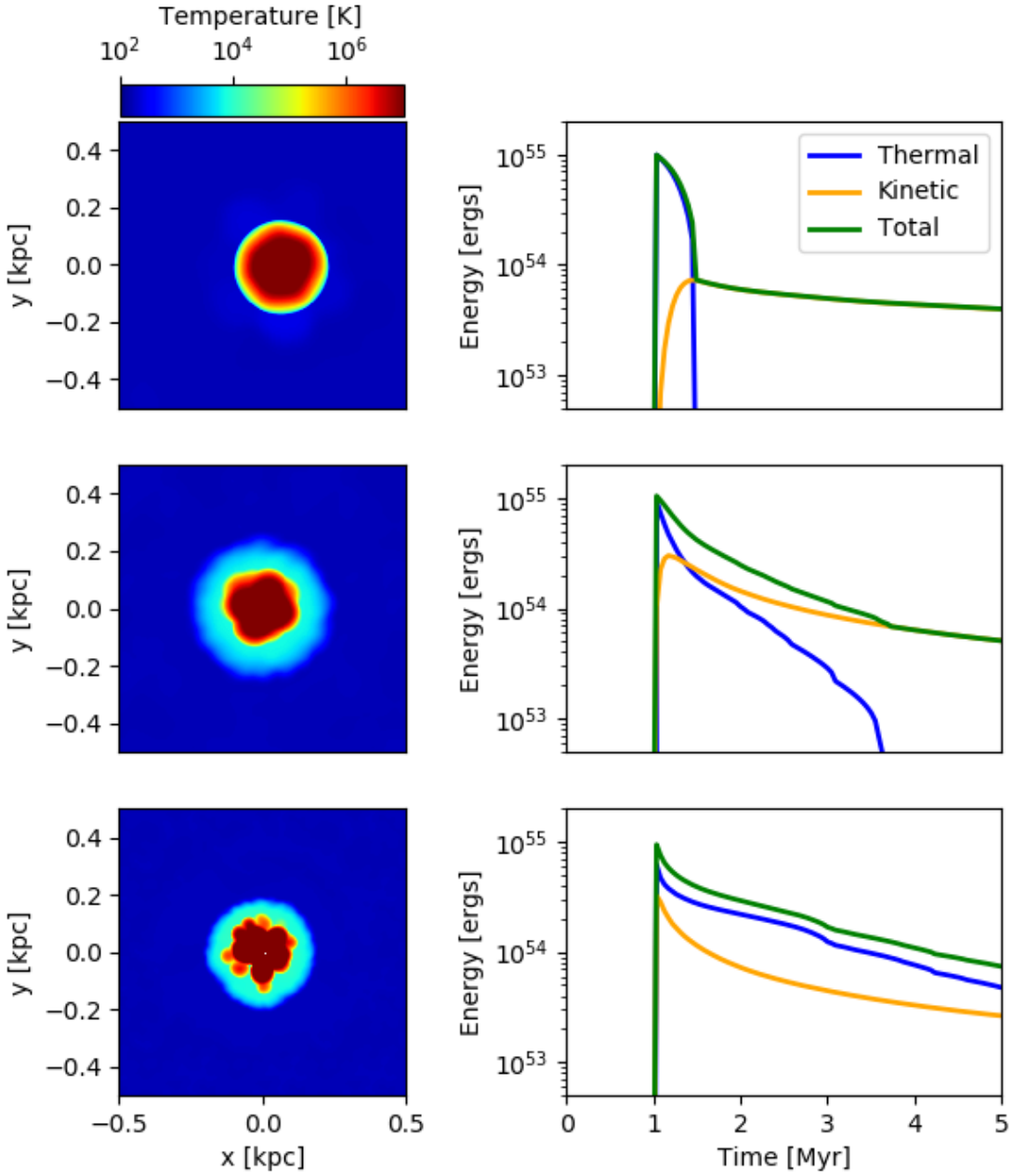

FIGURE 3.8: Test of a single thermal energy-dump feedback event at several resolutions. The first column shows a temperature slice of the feedback event. The second column shows the energy added to the gas over time. Top row is lowest resolution and each subsequent row has 8 times as many particles.

The AMR criteria refines any cell with mass greater than 10684 $M_{\odot}$, up to a maximum of 13 levels of refinement, giving a minimum cell size of 73.2 pc.

Figures 3.9 and 3.10 show the time evolution of gas density in each galaxy, projected along the z and x axis respectively. In contrast to the previous section, many differences can be seen between the two galaxies. The galaxy with no feedback has less gas overall, because a high fraction of it is used in star formation. The gas it does have is very concentrated into small clumps. The galaxy with delayed cooling feedback has more gas in the ISM and it is more evenly distributed. Additionally bubbles created from individual feedback events can be seen in the gas. The delayed cooling galaxy also has large vertical outflows of gas, reaching up to tens of kpc above the disk, something the simple feedback model was unable to produce.

Because of the higher star formation efficiency, each galaxy immediately begins forming stars very quickly. In the no-feedback case, the high star-formation rate continues, and then declines as the galaxy begins to run out of gas. In only 400 Myr roughly 80 % of the gas has been converted into stars. The galaxy with the simple feedback model has a somewhat limited star formation rate, but has a second burst in star formation and continues to remain several times greater than a galaxy run with a lower star formation efficiency. The SFR of the delayed cooling galaxy quickly drops to levels of the original galaxy run with a lower efficiency and remains there. This shows that the delayed cooling feedback model is clearly effective in limiting star formation. This is summarized in Figure 3.11 which plots the star-formation rates of each galaxy over time.

3.6 A Quick Recap

This chapter has presented several simulations of galaxies using a variety of methods, and placed some restrictions on which models are appropriate to use in which situations. Firstly, we found the minimum resolution requirement to accurately simulate a disk galaxy is the scale height of the disk. Without resolving the scale height, information along the z-axis is lost and results are nonsensical. Of course, if one wishes to study individual clouds within the ISM, that will require resolutions much higher than this. Next, we confirm previous results that using periodic boxes to simulate

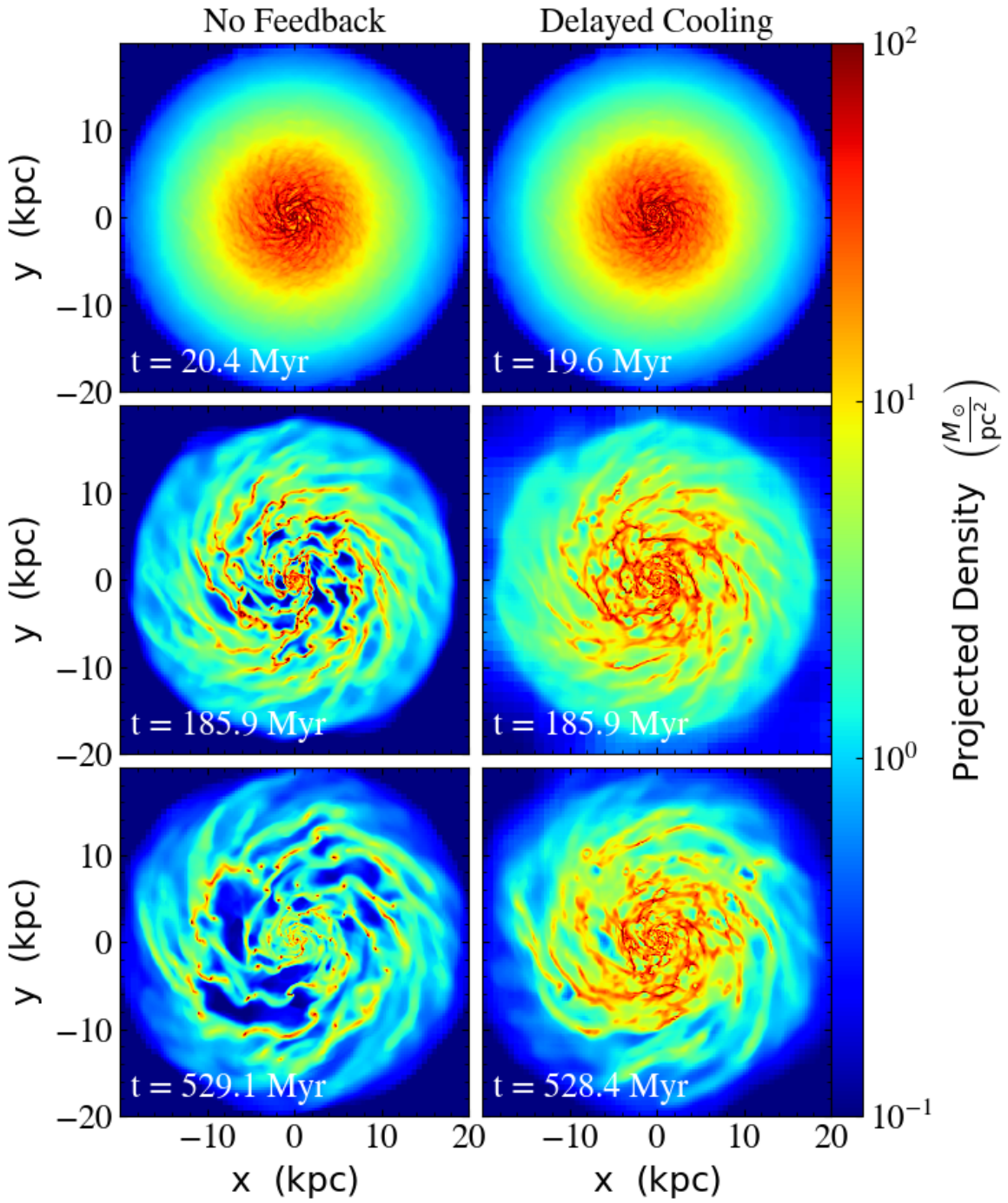

FIGURE 3.9: Time evolution of simulated galaxy with no stellar feedback (left column) and with delayed cooling feedback (right column). Each panel shows a projection of the gas density along the z-axis.

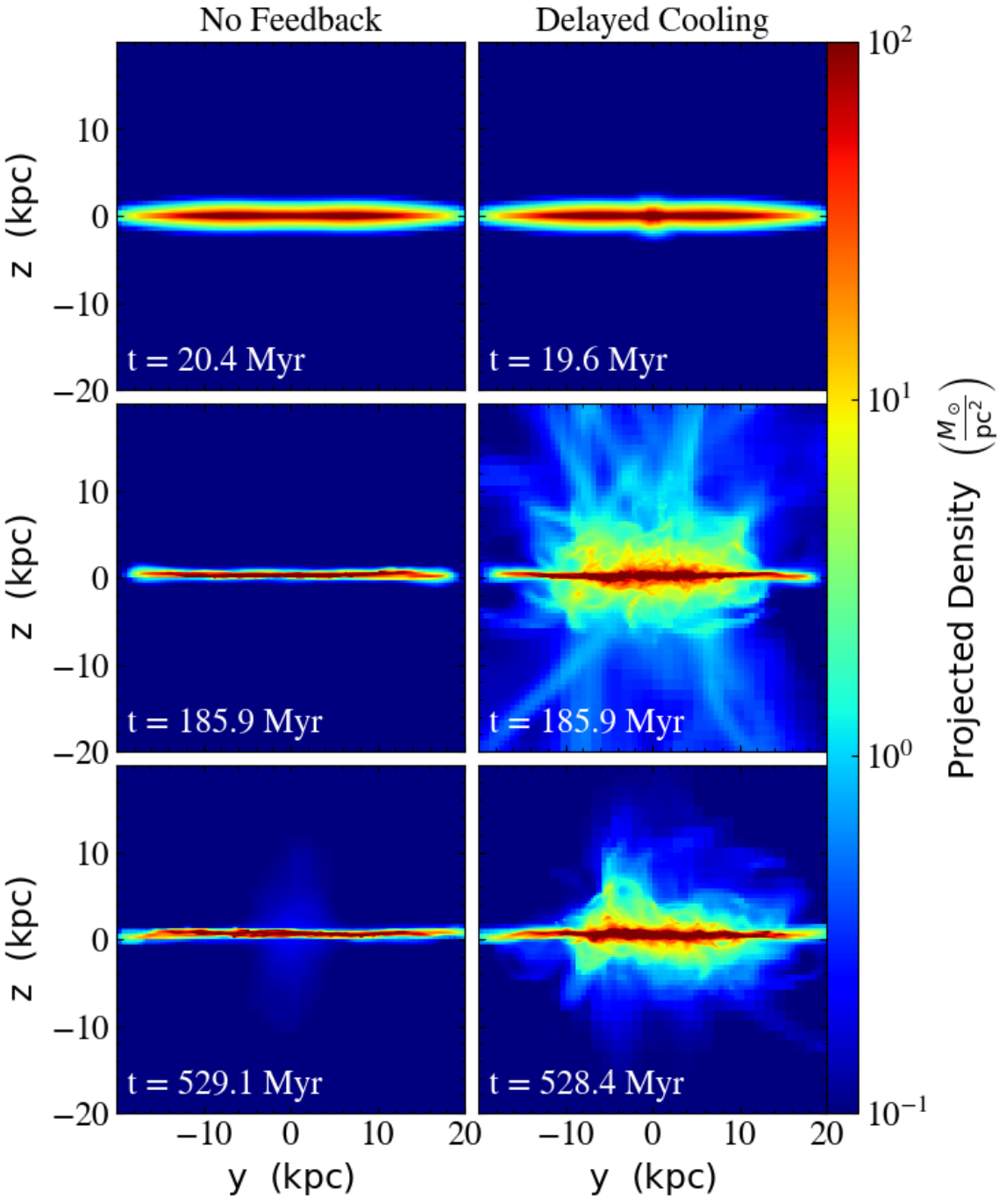

FIGURE 3.10: Time evolution of simulated galaxy with no stellar feedback (left column) and with delayed cooling feedback (right column). Each panel shows a projection of the gas density along the x-axis.

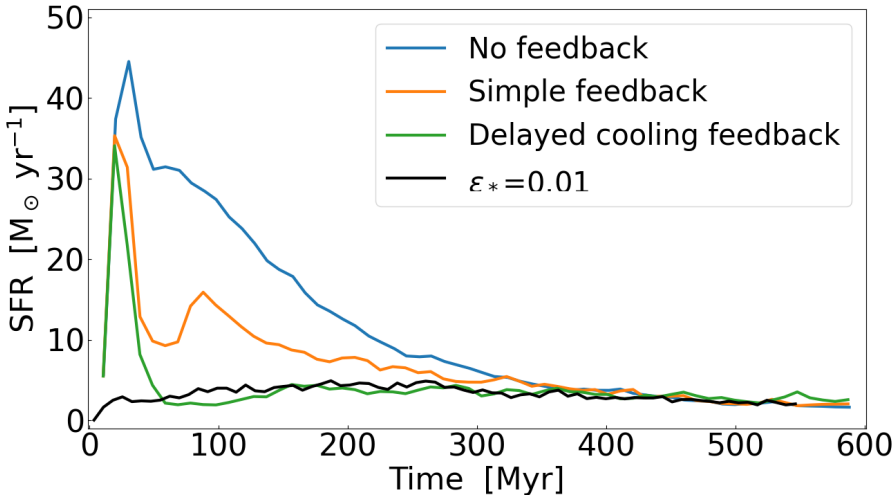

FIGURE 3.11: Star formation history of simulated galaxies with different feedback models. All galaxies have a star formation efficiency of $\epsilon_* = 0.1$ except for the black line.

the ISM of a galaxy does not realistically predict outflows or the star formation cycle, due to gas repeatedly exploding and oscillating along the z-axis, while not being able to escape horizontally (Martizzi et al. 2016b). We also find simple stellar feedback models fail to be effective due to a lack of numerical resolution, but increasing the resolution enough to counteract this is simply infeasible in galaxy simulations. Using a different feedback model can circumvent the problem and regulate star-formation more realistically. Using all these considerations, the next chapter continues with the inclusion of magnetic fields, and their interplay with these models and resolutions. All of our following simulations use the delayed cooling feedback model in isolated galaxy disks, with resolutions equal to or greater than those used in this chapter.

Chapter 4

Magnetohydrodynamic (MHD) Galaxies

Now that we have developed a framework for how to best simulate galaxies, we will continue by adding magnetic fields to the simulations and testing their effects. As discussed in Section 1.4.5, galactic magnetic fields have been known to exist for many decades, and many theories predict they play an important role galaxy disks and the ISM. A key goal will be to test the role MHD and the dynamo effect plays in generating and sustaining turbulence as compared to feedback.

To simulate magnetic fields, we use the MHD solver in RAMSES, rather than the usual regular hydrodynamics solver used in the previous chapter. We continue to use the Agora isolated disk galaxy as the initial condition, with the addition of an initial toroidal magnetic field (see Section 2.4.2). The initial setup of the magnetic field can be seen in Figure 4.1. We conduct a total of four separate simulations in this section, simulating the galaxy at two different resolutions and with or without magnetohydrodynamics. The high resolution simulations are conducted with a minimum grid cell size of 9.15 parsecs, 8 times smaller than our previous simulations, which corresponds to a mass resolution 512 times smaller at 21 $M_\odot$. The high resolution runs are able to reach much higher densities so the star formation threshold density is increased from 10 m_p/cm^{-3} to 100 m_p/cm^{-3}. Such a large jump in resolution is used to ensure the small scale dynamo is being resolved (R. Teyssier, private communication). Due to the computational constraints of the higher resolutions, those runs were only evolved for 135 Myrs. Our analysis of the high resolution galaxies are all done on the final

snapshot of the galaxy. All of the following simulations use delayed cooling feedback, a Jeans pressure floor, and heating and cooling rates from GRACKLE. The lower resolution run done with hydrodynamics is the run used in the previous chapter. The four setups used are summarized in table 4.1.

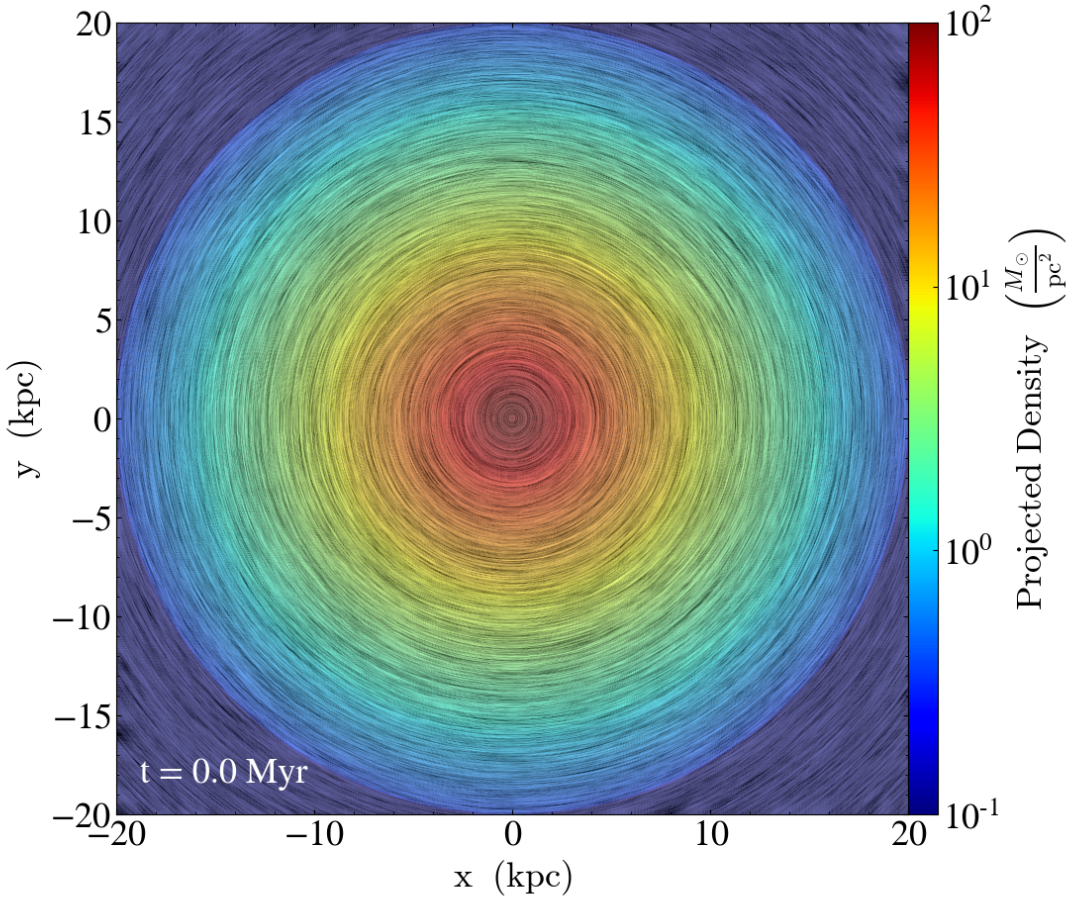

FIGURE 4.1: Density projection of the IC used for all simulations in this chapter. The lines show the magnetic field lines, created via a line integral convolution. The magnetic field strength scales as $B \propto \rho^{2/3}$

4.1 Low resolution results

We first present the results from simulations done at the same resolutions as the previous chapter. The time evolution of the MHD galaxy as compared to the hydro

Simulation	Minimum grid size (pc)	Refinement Mass ($M_\odot$)	ρ_{star} (m_p/cm^{-3})	Solver
hydro_lowres	73.2	10684	10	Hydro
mhd_lowres	73.2	10684	10	MHD
hydro_highres	9.15	21	100	Hydro
mhd_highres	9.15	21	100	MHD

TABLE 4.1: A summary of different parameters used in the simulations

galaxy can be seen in Figures 4.2 and 4.3, which show z and x projections respectively. Neither galaxy appears much different from the other. Both have vertical outflows of gas, and an ISM that remains evenly distributed throughout the lifetime of the galaxy. The MHD galaxy does not display any immediate behaviour that stands out from the hydro galaxy.

The lack of effects from MHD is also apparent in the star formation histories, as shown in Figure 4.4. This figure also shows the results from two galaxies simulated without any stellar feedback. As expected, the use of feedback has a drastic effect on the star formation rate, however the magnetic fields do not seem to make a difference. Even when both magnetic fields and feedback are combined together, there is no significant effect on the galaxy, contrary to results by Rieder and Teyssier (2016), who suggested that supernova feedback can create turbulence and cause the small-scale dynamo to emerge. However those simulations used resolutions of 18 pc, and for that reason we now go to higher resolution to investigate whether magnetic fields continue to play a minor role.

4.2 High resolution simulations

Time evolution of the high resolution simulations can be seen in Figures 4.5 and 4.6. Because the high resolution runs were run for a shorter total duration, the time difference between the snapshots shown is less than in previous figures. Similarly to the low resolution runs, the galaxy has a burst of star formation at the beginning of the run. The star formation begins in the center of the galaxy as the gas is compressed vertically and moves its way outwards in a ring. After the initial burst of star formation the ISM

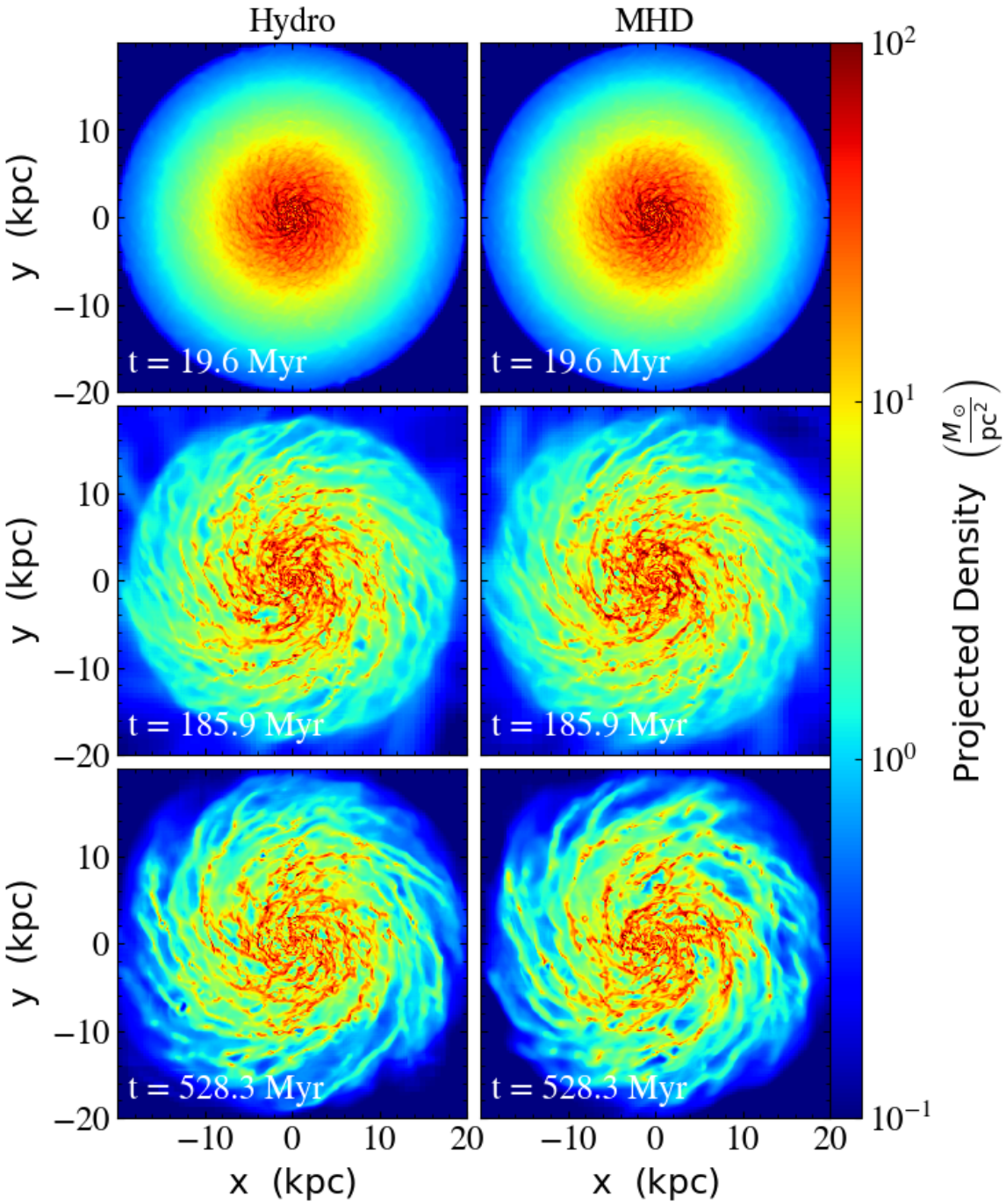

FIGURE 4.2: Time evolution of low resolution galaxy with hydrodynamics (left column) and MHD (right column). Each panel shows a projection of the gas density along the z-axis.

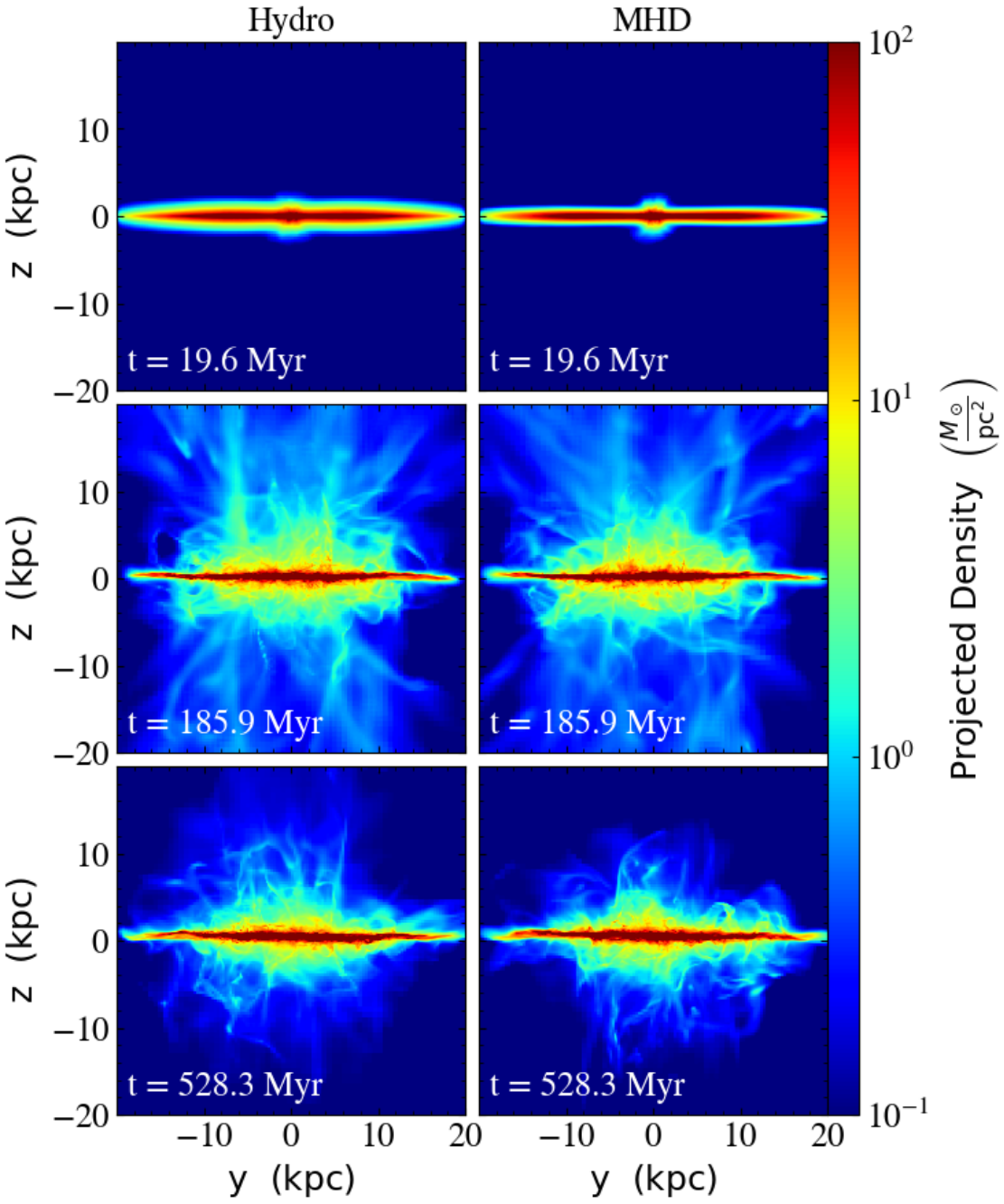

FIGURE 4.3: Time evolution of low resolution galaxy with hydrodynamics (left column) and MHD (right column). Each panel shows a projection of the gas density along the x-axis.

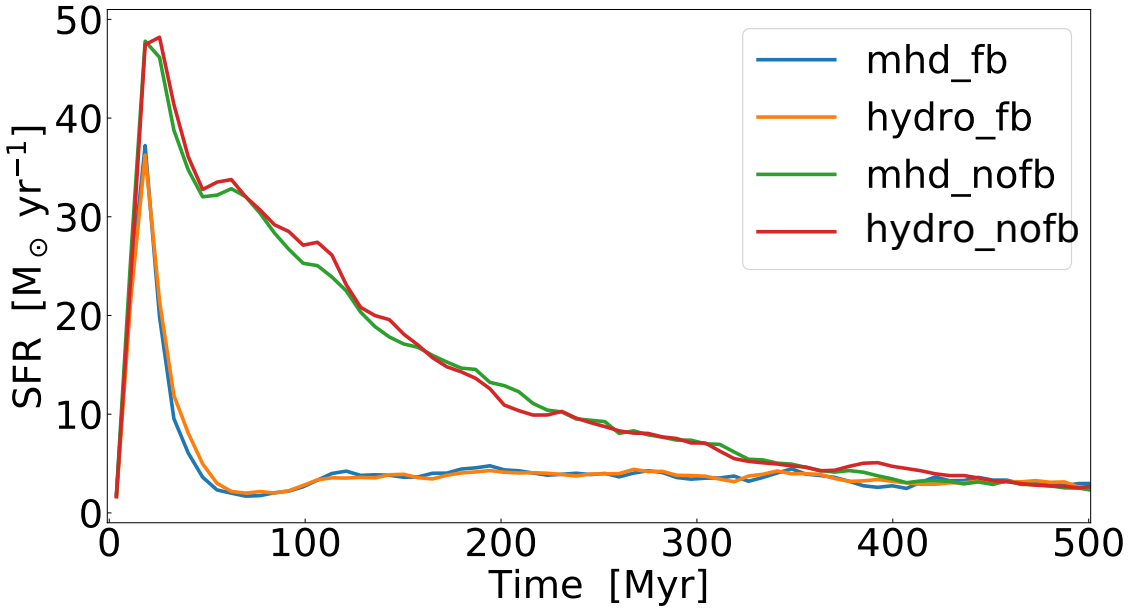

FIGURE 4.4: Star formation history of simulated galaxies with different feedback models. All galaxies have a star formation efficiency of $\epsilon_* = 0.1$.

inside the ring reaches an equilibrium where star formation and feedback continues, but at expected rates. In the MHD run the ring can be seen to have much more well defined edges, and its radial extent lags slightly behind the hydro run.

Large X-shaped outflows of gas characteristic of starburst galaxies can be seen in Figure 4.6. However the star formation burst has ended by 40 Myrs into the run. In the MHD run the outflows of gas have a smaller vertical extent in the final snapshot, suggesting the gas is falling back down faster than in the hydro run. In the earliest snapshot, the MHD run has more dense gas that has been dragged up into the halo than in the hydro run. Figure 4.7 shows the central region of each high resolution galaxy. In the hydro galaxy, the blue under-dense feedback bubbles are qualitatively larger than in the MHD case, suggesting magnetic fields couples the feedback to the mass, meaning feedback events drag more gas with them. The hydro galaxy may have more effective feedback, but it carries less mass.

The star formation histories of all four galaxies are shown in Figure 4.8. For the first time there is a difference between the MHD and the hydro galaxy. Compared

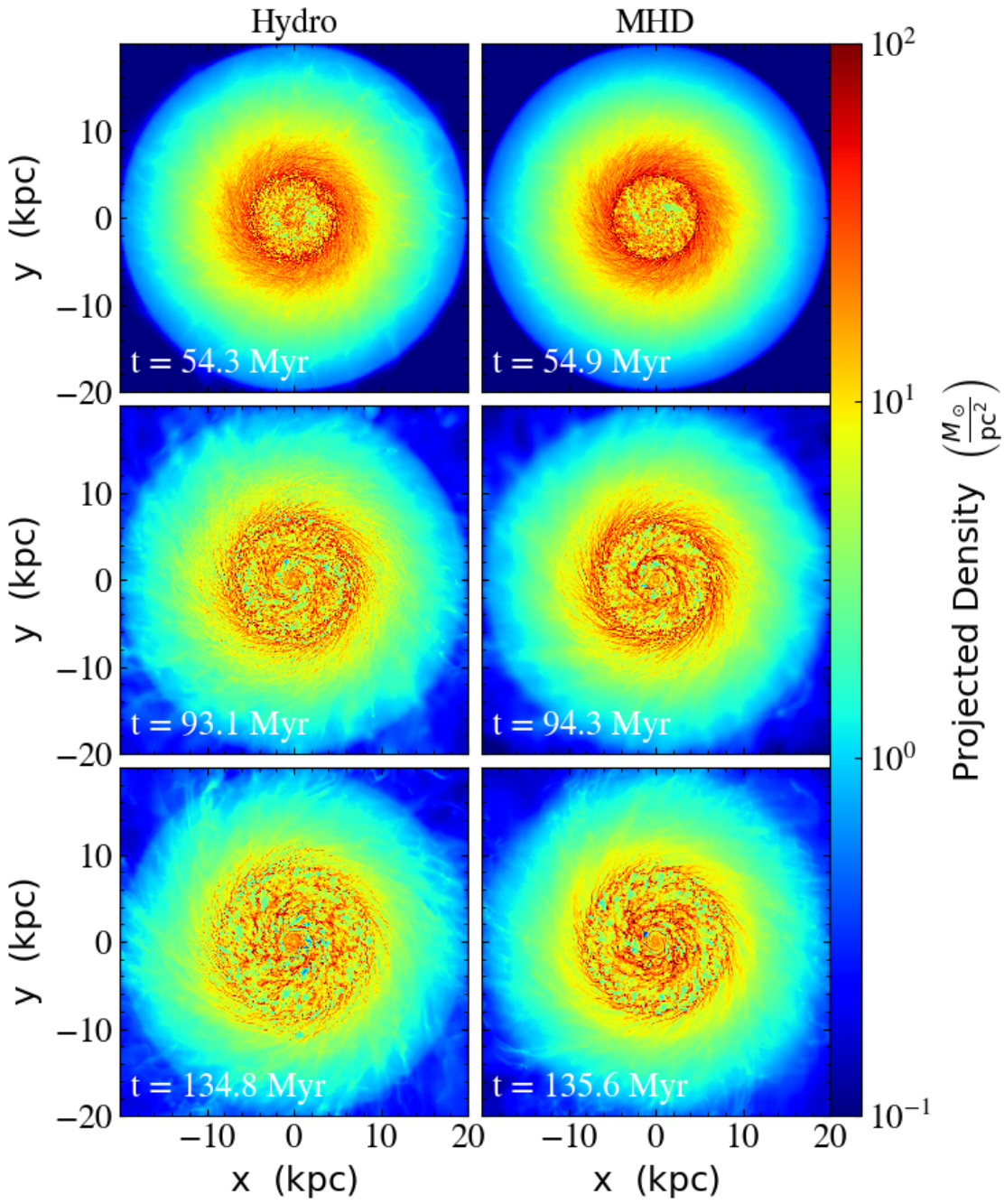

FIGURE 4.5: Time evolution of high resolution galaxy with hydrodynamics (left column) and MHD (right column). Each panel shows a projection of the gas density along the z-axis.

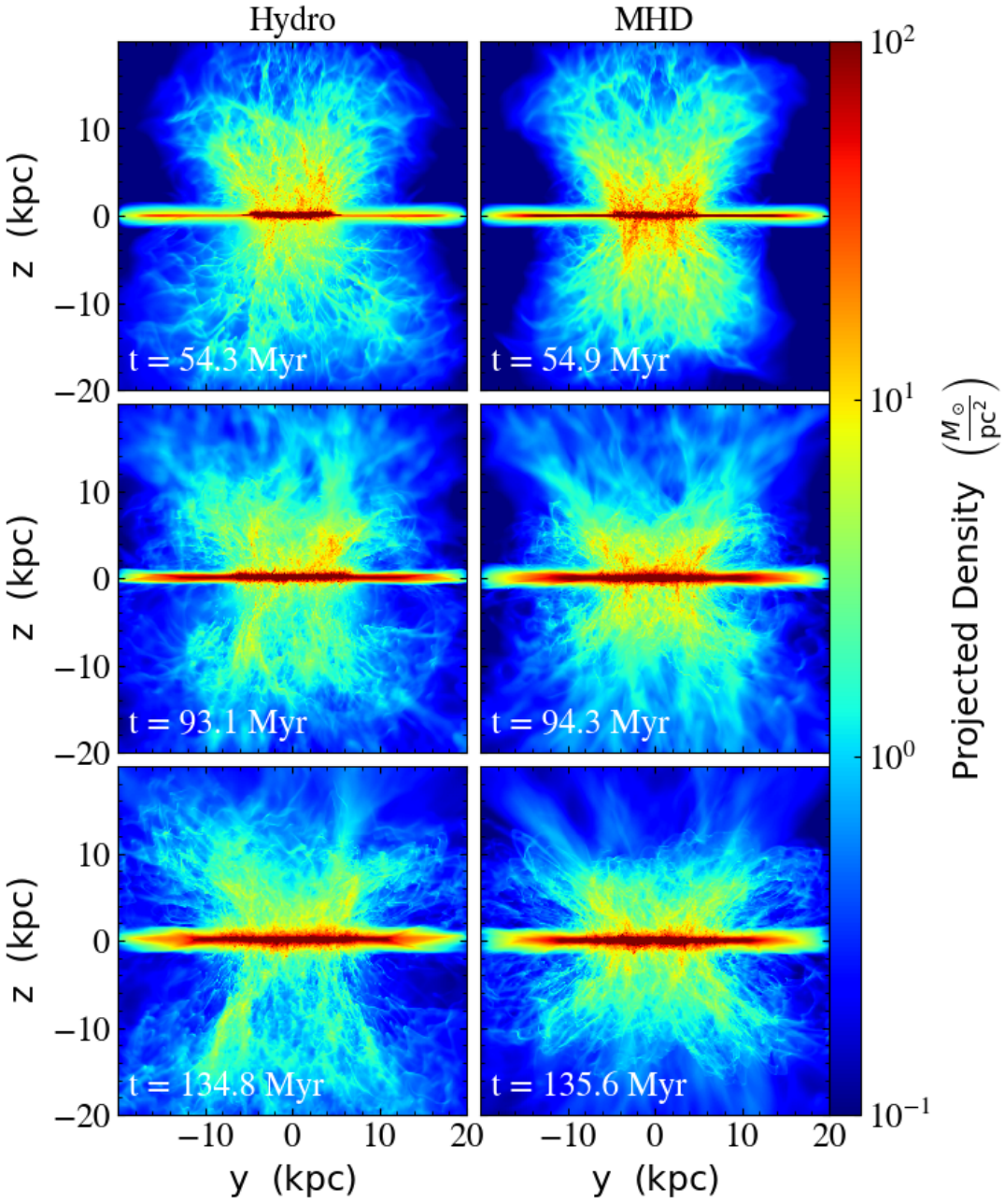

FIGURE 4.6: Time evolution of high resolution galaxy with hydrodynamics (left column) and MHD (right column). Each panel shows a projection of the gas density along the x-axis.

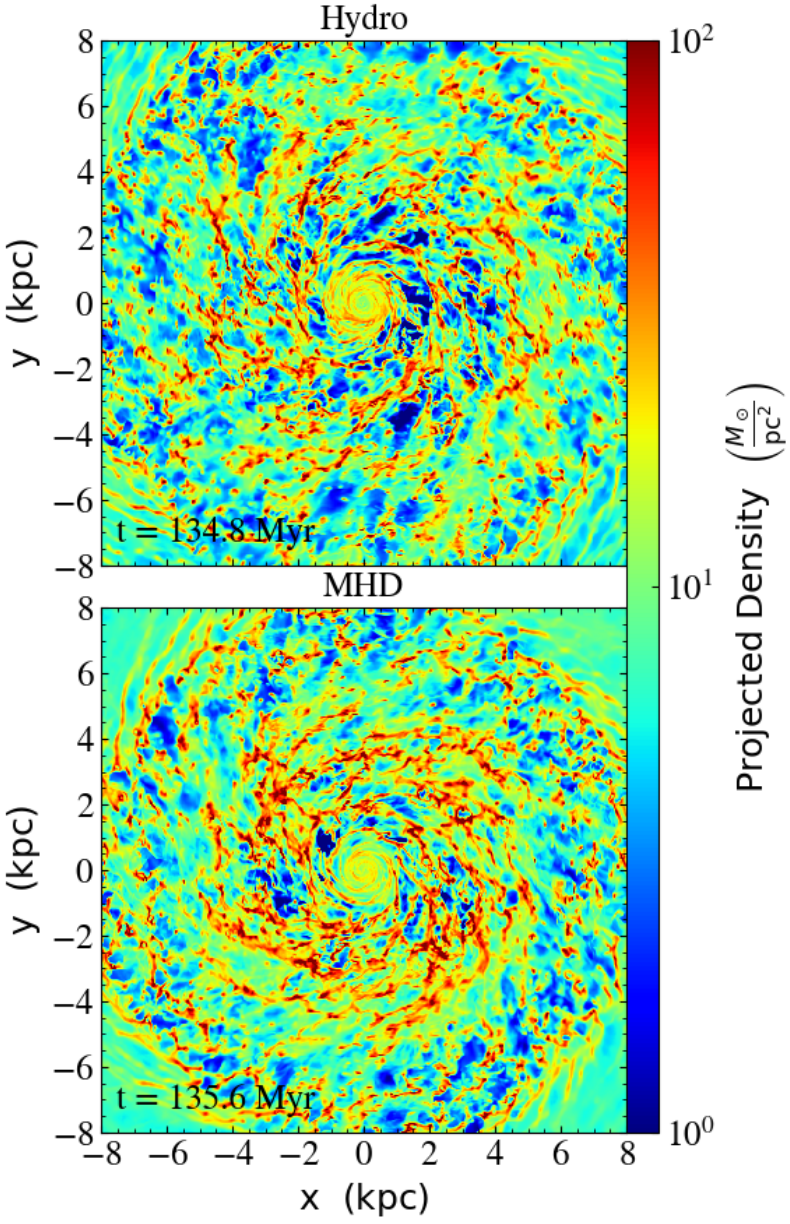

FIGURE 4.7: Central 8 kpc of each high resolution galaxy in the final snapshot. Each panel shows a projection of the gas density along the z-axis.

to the hydro run, the high resolution MHD galaxy has a slightly lower star formation rate for first 100 Myr of the run. It also shuts star formation down after the the initial starburst faster than the hydro galaxy. When increased to high resolution, magnetic fields seem to begin to have an effect on the behaviour of the galaxy. From the star formation histories and density projections alone, the differences may seem small, but we now do a much more in depth analysis of the behaviour of each galaxy to determine exactly what is going on.

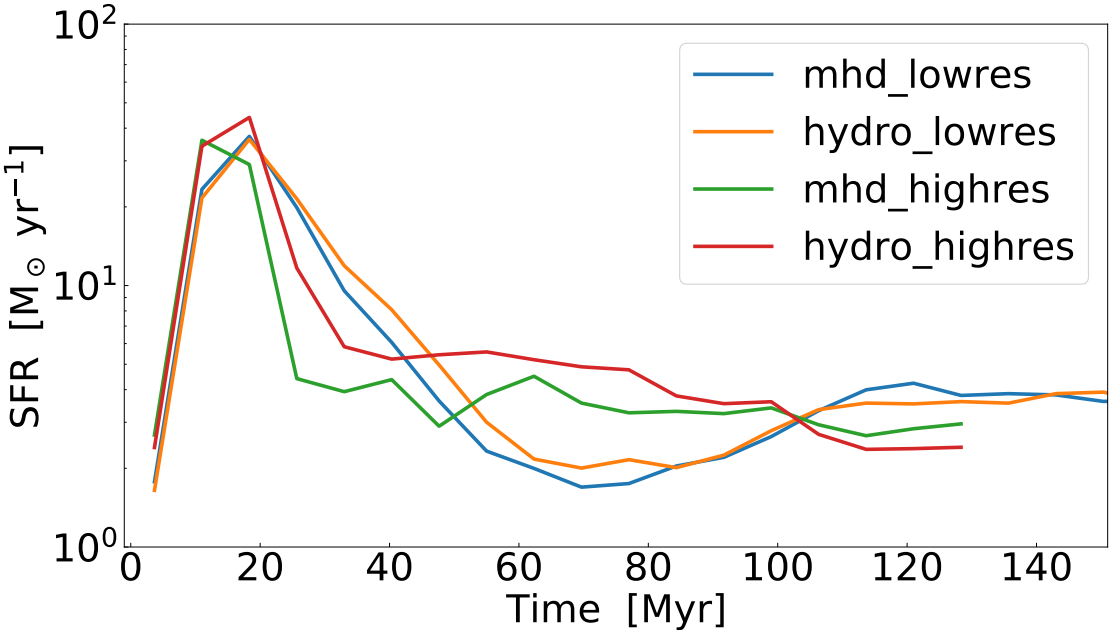

FIGURE 4.8: Star formation history of the four simulated galaxies. All galaxies have a star formation efficiency of $\epsilon_* = 0.1$.

4.3 Differences Between the Galaxies

The star formation of a galaxy is largely controlled by its supply of dense gas. Figure 4.9 is a histogram of gas densities in each galaxy. The low resolution galaxies have a distribution that peaks around 1-5 m_p/cm^{-3}, meaning most of the gas exists in the cold/warm neutral medium. The distribution descends fairly smoothly into the lower density ionized mediums, and drops off quickly above the star formation threshold $\rho_{star} = 10$ m_p/cm^{-3}, at this resolution GMCs ($\rho_{gas} > 100$ m_p/cm^{-3}) are not resolved at all. Both of the high resolution galaxies have a double-peaked distribution with almost

equal amounts of gas existing in the cold and warm ISM, matching the expectations of a two-phase ISM from Field et al. (1969). The high resolution galaxies have a higher star formation threshold so they extend into the densities of GMCs and begin to resolve them. Strikingly, there is a difference between the MHD and hydro galaxy at high resolution that does not exist at lower resolution; the MHD galaxy has less mass in the cold phase, and more gas in the warm phase. This would explain the slightly reduced star formation rate because there is simply less fuel for star formation.

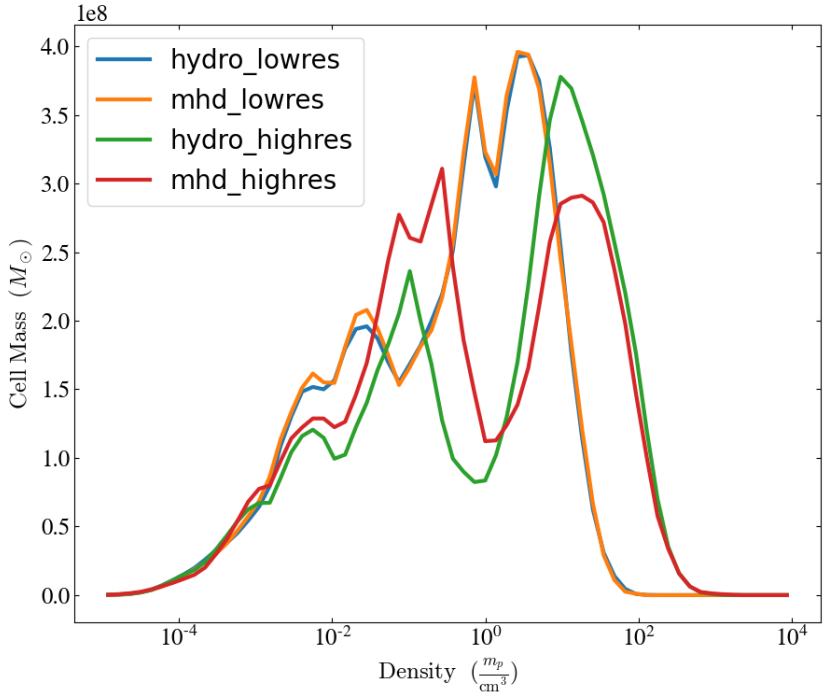

FIGURE 4.9: Density histogram of gas in each simulated galaxy, plots the total amount of gas mass at a given density.

The scale height of each galaxy is shown in Figure 4.10. All of the galaxies have the lowest scale height in the center and flare up at farther radii. Both of the high resolution galaxies have large scale heights at ∼13 pc where the ring of star formation continues to move outwards. Interestingly, both hydro galaxies have roughly the same scale heights, while the MHD galaxies differ. The low resolution MHD galaxy has a smaller scale height than all the others, and the high resolution MHD run has the highest scale height, remaining around 300 pc high out to 10 kpc, matching closely

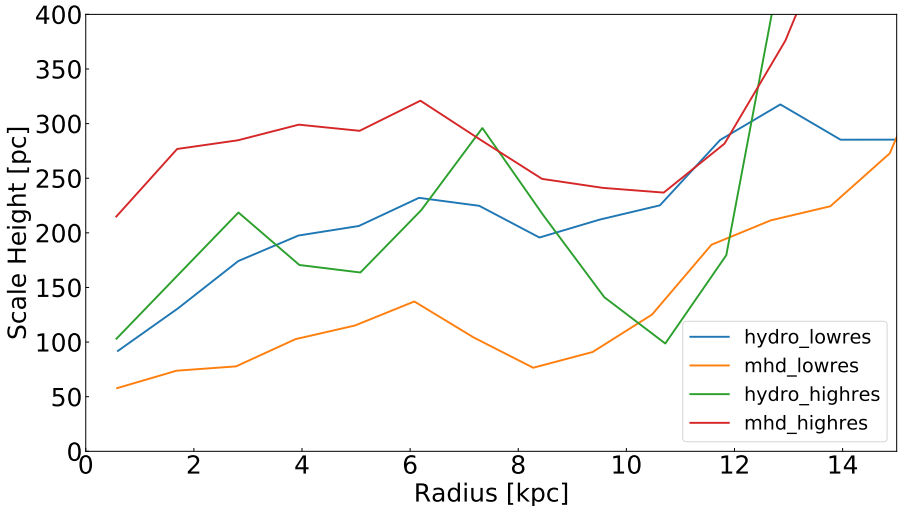

FIGURE 4.10: Scale height of each galaxy vs radius at final time of 135 Myr.

with values for the thin disk of the Milky way of 300-400 pc (Sparke and Gallagher 2007). The large scale height in the high resolution MHD galaxy implies there is higher pressure supporting it, which is particularly impressive given it has a lower SFR. While the enhanced scale height could be due to magnetic fields dragging more gas along in outflows, it could also be from a mechanism proposed in Körtgen et al. (2019), that magnetic fields can drag gas several hundreds of parsecs above the midplane via the Parker instability independent of feedback.

Now that we have shown the gas in the high resolution galaxies is behaving differently, the natural next question to ask is why. What is keeping the gas in the warm ISM of the MHD galaxy and puffing up the scaleheight? A good way to examine this is to look at what pressure is supporting the gas. A density-pressure phase diagram for each galaxy is plotted in Figure 4.11. Like Figure 4.9, this is a histogram, but it has an added dimension of pressure along the y-axis. The gas settles into what is known as a cooling curve that is controlled by the heating and cooling processes. There is a diagonal line that extends across the plot which is warm gas sitting at 10^4 K, and once it reaches a density of around 1 m_p/cm^{-3}, it transitions into the cold ISM and GMCs where the pressure is relatively lower. The diffuse blue region on the left of the plot is the hot gas created by supernovae. Both high resolution runs have significantly more hot gas than the low resolution runs, despite having less total gas at

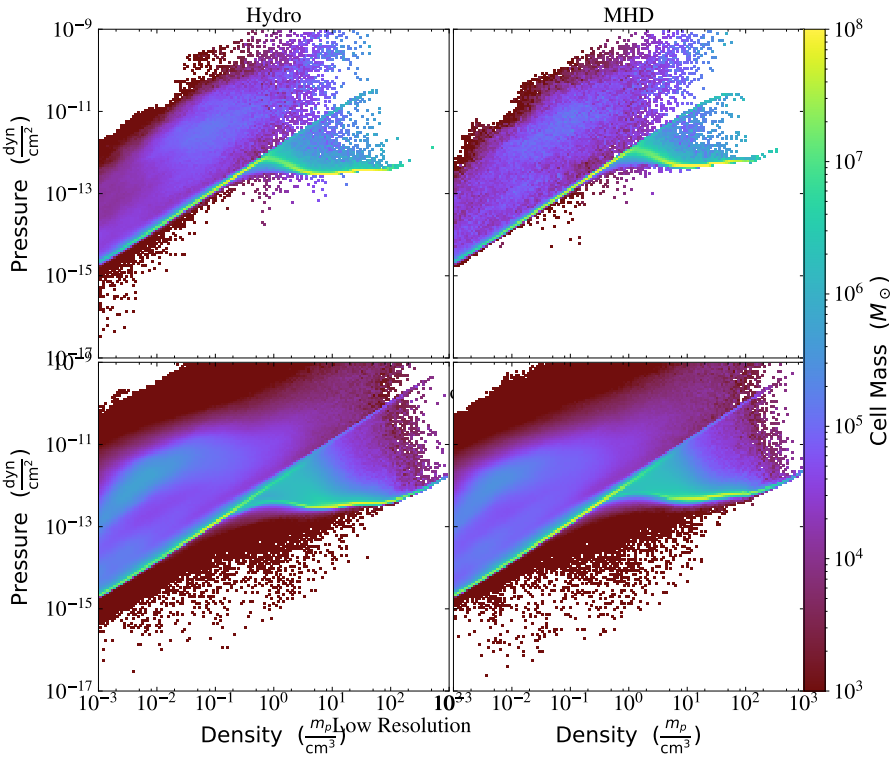

FIGURE 4.11: Two-dimensional density-pressure histogram for each galaxy. The colour scales with the log of the total mass in each bin. Shows both low resolution run (top row), and high resolution runs (bottom row).

those densities. The main differences visible on this plot are between the resolutions, the addition of MHD does not seem to play an important role in the thermal pressures in the gas. However, thermal pressure is not the only kind of pressure supporting the gas. Magnetic fields exert a pressure on the gas of the form

$$P_{mag} = B^2/8\pi \tag{4.1}$$

in cgs units. Turbulent motions can also support the gas and provide a turbulent pressure that can be given by

$$P_{turb} = \rho_{gas} v_z^2 \tag{4.2}$$

which is equivalent to the kinetic energy density of just the z-component of velocity (Rieder and Teyssier 2017).

Figure 4.12 shows the distribution of all three types of pressure in the MHD galaxies. In high density gas, thermal pressure is never the dominant support. In fact turbulence dominates the support almost everywhere. The magnetic pressure become stronger than thermal pressure at densities of around 10 m_p/cm^{-3}. The thermal pressure is distributed more tightly because it is controlled by the equilibrium established between the heating and cooling functions, whereas the magnetic and turbulent pressures vary greatly at a given density because they depend directly on the values of the magnetic field or velocity.

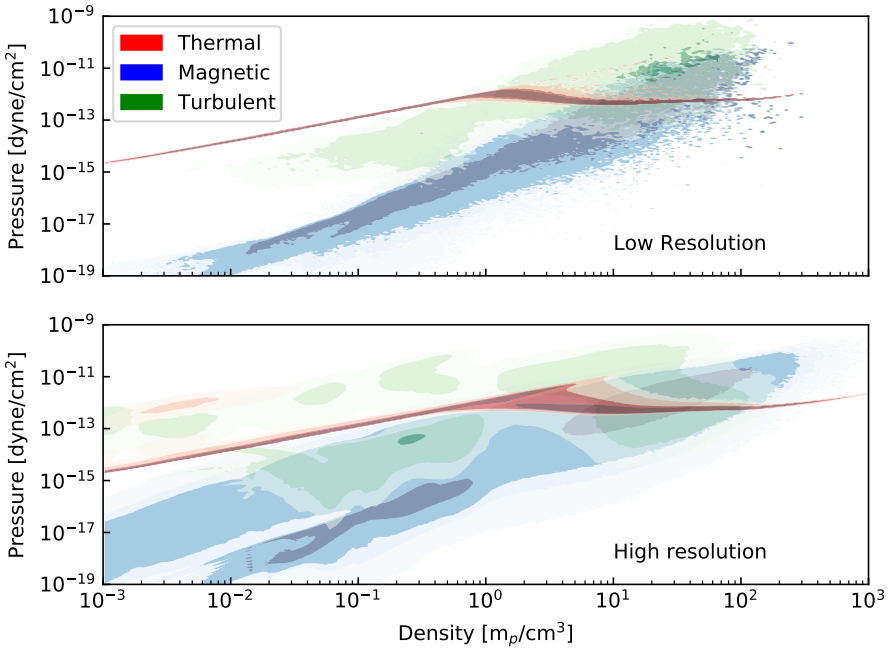

FIGURE 4.12: Density-pressure contour diagram, shown for both MHD galaxies. The colour scales linearly with the total mass enclosed in the region.

A simplified but easier to interpret version of the phase diagram can be seen in Figure 4.13, which compresses the pressure distributions to a single line, and also includes the hydro galaxies. Also plotted in this figure is the Jeans pressure floor. In both low resolution galaxies, the Jeans floor begins to dominate around the star formation threshold density, meaning that in all star forming gas the artificial Jeans floor is the main form of support. This is not true in the high resolution galaxies, partly because the Jeans floor is smaller at higher resolutions, but also because the

turbulent pressure is enhanced. This is especially true in the MHD high resolution galaxy, where the turbulent pressure dominates over every other pressure even up to the highest densities. The magnetic pressure also play a greater role in high resolution galaxy; it is stronger than the thermal pressure in all of the star forming gas, compared to the low resolution MHD galaxy where this is only true for a small fraction of star forming gas at the highest densities. Previous results by Rieder and Teyssier (2017) show that magnetic pressure saturates at about 1% the strength of thermal pressure on average, but can dominate in localized regions. We can see that the regions of where magnetic pressures dominates is in high density gas, and it dominates more the higher the density.

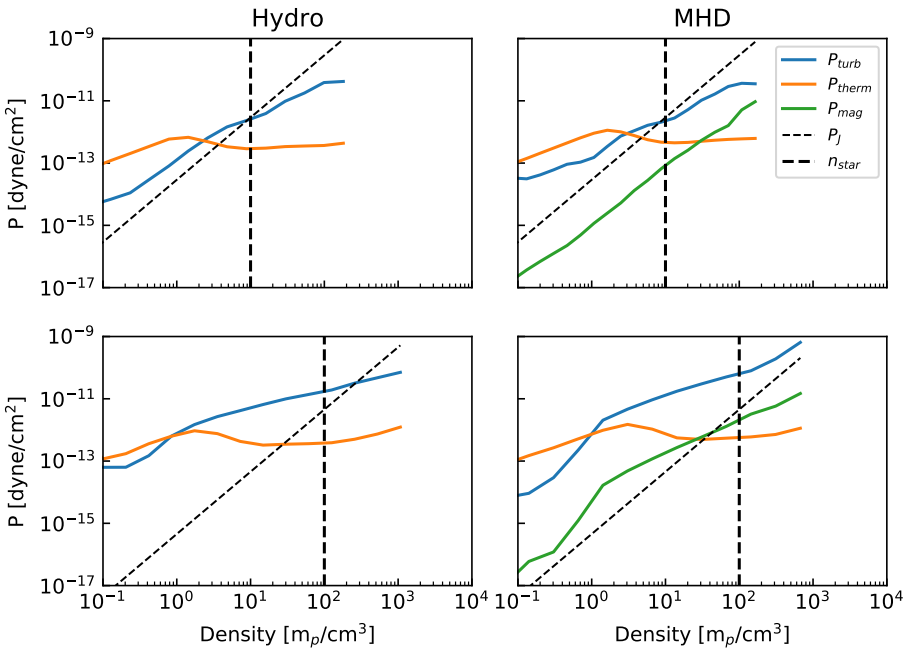

FIGURE 4.13: Median pressure of each type at a given density for low resolution galaxies (top row), and high resolution galaxies (bottom row). Also plotted are the Jeans pressure floor (P_J), and the star formation threshold density ρ_{star}.

4.4 Motions in the Gas

We have explored the differences between the distributions of gas in each galaxy, but we now investigate differences between the motions of the gas in each Galaxy. Figure 4.14 shows the vertical motions of gas in each galaxy during the final snapshot. In all cases, above the disk of galaxy there are inflows and outflows of gas moving at speeds of order a hundred km/s. Outflows likely come from supernovae in the disk and the inflows come from gas falling back down onto the galaxy. Because the simulations only ran for 135 Myr there may still be leftover motions from the initial starburst as well.

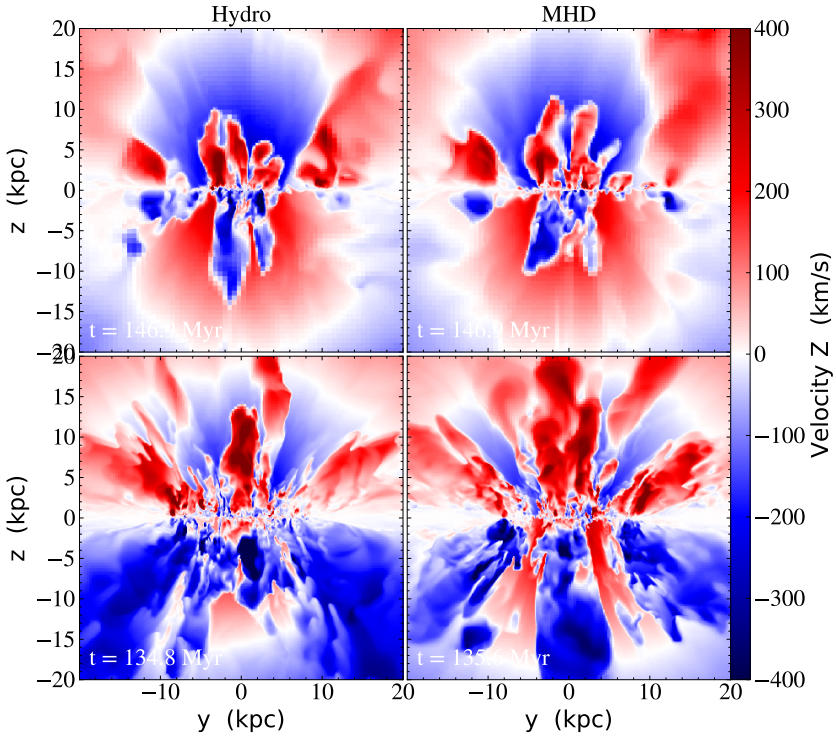

FIGURE 4.14: Slice of z-velocity in y-z plane for each galaxy. Top row shows low resolution galaxies and bottom row shows high resolution.

As perhaps expected, the low resolution hydro and MHD galaxies look essentially the same. The vertical outflows don't reach higher than ∼10 kpc in either of the low resolution runs. In the high resolution galaxies the outflows reach well past 20 kpc above the midplane, and have much higher velocities than the low resolution galaxies. This could partly be a result of reduced artificial viscosity at higher resolutions, but

is due to star formation being more clustered because of the higher star formation threshold density. Supernova that occur in clusters will combine their effects and have more violent outflows.

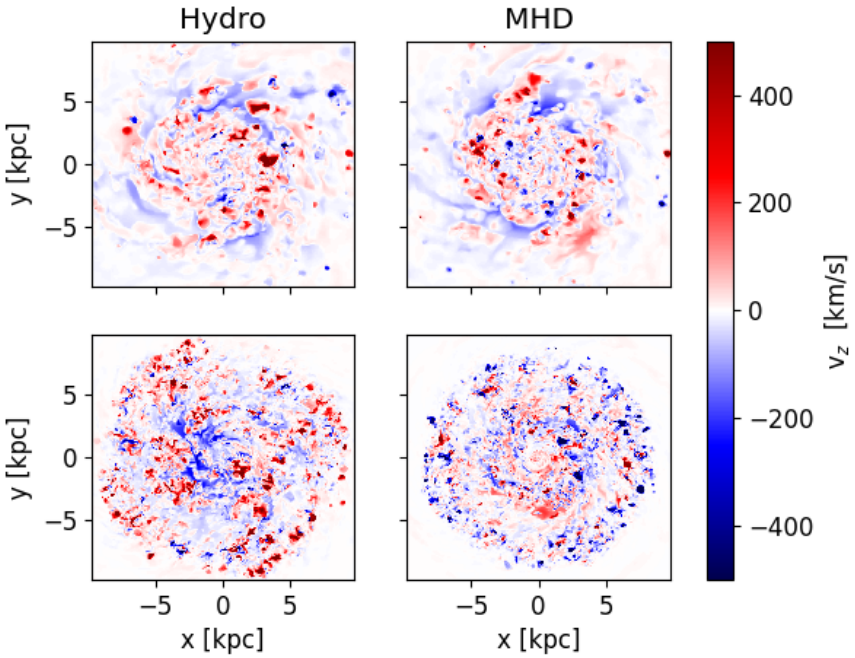

FIGURE 4.15: Slice of z-velocity in the midplane of each galaxy. Top row shows low resolution galaxies and bottom row shows high resolution.

The vertical motions of gas in the midplane are shown in Figure 4.15. Individual feedback events are visible in all of the galaxies as small regions with high z-velocities. Note that the high velocities on this plot mostly show outflows of gas out of the disk, the turbulent motions within the gas are of the order 10 km/s and will not show up well. To characterize the turbulent motions in the midplane we now go to Fourier-space, which will also help describe the scales at which the motions occur on. Figure 4.16 shows the 2D Fourier transform of the z-velocity maps. The Fourier transforms all look similar, with the most power occurring at large scales, with the exception of the high resolution MHD run which looks slighty more diffuse. Using the Fourier transform we can construct the power spectrum of the z-velocity field, defined as:

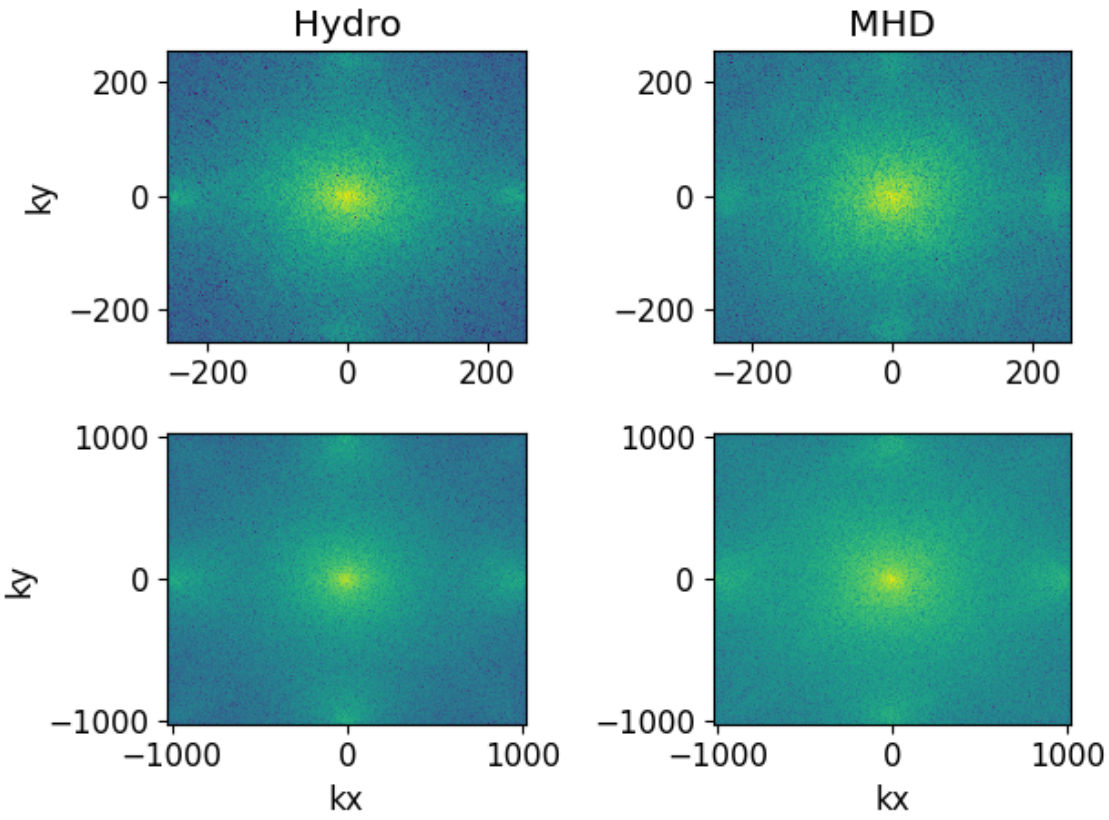

FIGURE 4.16: 2D Fourier transforms of z-velocities in the midplane of each galaxy. Created using the maps in Figure 4.15. The wavenumbers k_x and k_y are shown in units of grid cells. Colour scales with the log of the value at each point. Top row shows low resolution galaxies and bottom row shows high resolution.

$$P(\vec{k}) = \tilde{v_z}(\vec{k}) \cdot \tilde{v_z}(\vec{k})^* \tag{4.3}$$

Where $\tilde{v_z}(\vec{k})$ is the Fourier transform of $v_z(\vec{x})$, $\tilde{v_z}(\vec{k})^*$ is its complex conjugate, and $\vec{k}$ is the wave vector. Then to obtain a one dimensional power spectrum we bin $P(\vec{k})$ in bins of $k = |\vec{k}|$ and divide by the number of points in the bin. The one dimensional power spectrum is shown in Figure 4.17. In all of the runs, most of the power is in the largest scales, where it is injected through galactic motions. The power then cascades down to lower scales through turbulence. This is similar to results from Rieder and

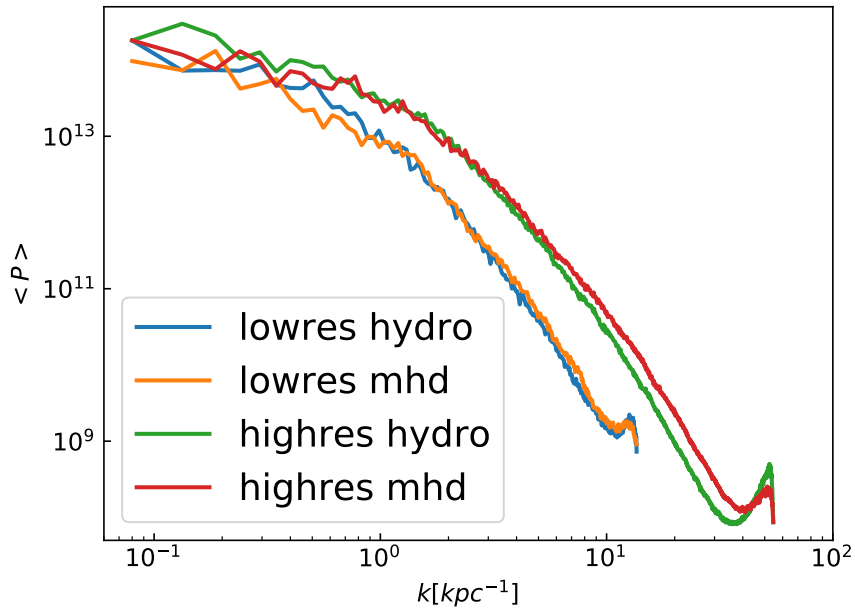

FIGURE 4.17: One dimensional power spectrum of the z-velocity field in the midplane of each galaxy. Created using Equation 4.3.

Teyssier (2016), but they did a Fourier transform on the 3D kinetic energy, while we looked only at the z-velocities in the midplane, resulting in a different power law slope. At the scales of a few grid cells there is an upturn that arises from a numerical bottlenecking effect (Lemaster and Stone 2009), which is an unphysical effect due to energy not being able to dissipate at the smallest scales. The low resolution runs have roughly the same power at every scale, but the in high resolution runs the MHD galaxy has increased power on small scales. It's worth noting that these are log axes so there is at least a factor of 2 more power on small scales in the MHD run. The difference between hydro and MHD begins to occur at scales around 100-500 pc, roughly the size of feedback bubbles. The enhanced power on small scales in the MHD run is clear evidence of enhanced turbulence that likely comes from magnetic fields coupling gas to feedback events.

4.5 Evolution of the Magnetic Fields

So far we have only begun to address how magnetic fields affect the evolution of the galaxy, but have ignored how the galaxy affects the evolution of the magnetic fields. Rieder and Teyssier (2016) showed that dynamo processes in the galaxy will ramp up magnetic field strengths, and the rate at which this happens is resolution dependent. At high resolutions the small-scale dynamo is better resolved and field strengths grow much faster. This is seen in Figure 4.18 which plots the total magnetic energy in each galaxy over time. In both runs there is an initial phase where of growth where the field grows very rapidly. This generates stronger fields in the high resolution run. Following that there is a second phase of slower growth where both runs have roughly the same rate of growth. In the low resolution run the field saturates at 400 Myrs, but in the high resolution run the fields have not yet saturated by the end of the simulation. Time evolution of the magnetic fields is also shown in Figures 4.19 and 4.20, which show slices of the magnetic fields plotted at various times. In the high resolution galaxy, the field strengths can be seen to be growing quickly in the outer disk, this is where the rapid growth seen in Figure 4.18 occurs. Within the ring of feedback the magnetic field forms in long snakelike filaments in the cold gas, corresponding to regions of high density seen in Figure 4.7. This can be especially seen in the Figure 4.21 which shows the central regions. There are very sharp edges in the field strengths along feedback bubbles, showing that fields are dragged out along with the gas.

Figure 4.22 shows a phase diagram of magnetic field strengths for the MHD galaxies at different times. The initial condition of the galaxy has magnetic field strengths that scale as $B \propto \rho^{2/3}$ but each galaxy quickly evolves to a slightly steeper power law, especially at high densities. The spread in field strengths at a given density increases with time. In the high resolution run the extra mass in the warm phase can be seen to have magnetic field strengths of 1-100 nG, and the relatively lower amount of gas in the cold ISM has field strengths of 1-100 μG

The field strengths are compared to observed magnetic field strengths from in the Milky Way (Crutcher et al. 2010) in Figure 4.23. The highest densities in our simulation start to overlap with the lowest densities required to observe magnetic field

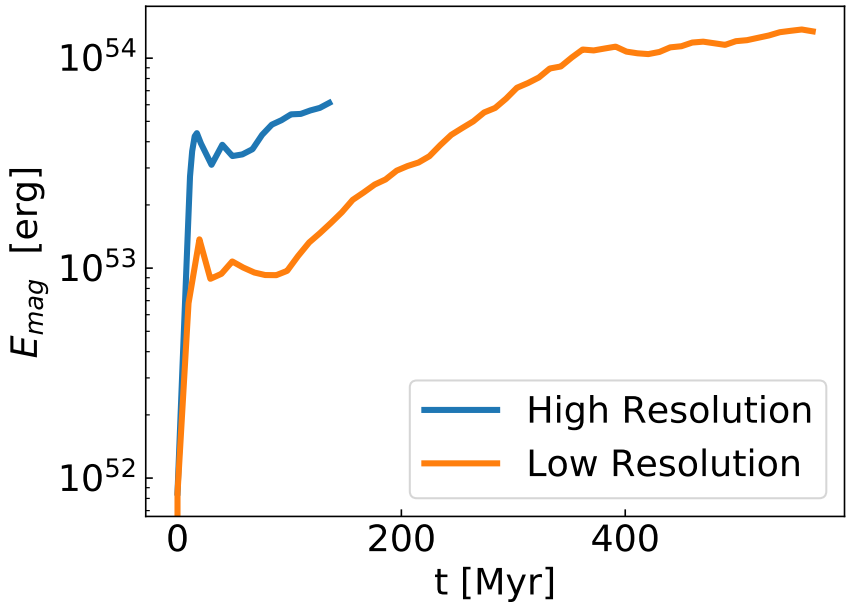

FIGURE 4.18: Total magnetic energy in each MHD galaxy vs time.

strengths. Our field strengths show good agreement within this regime, but it is unclear if that would continue higher densities. Crutcher et al. (2010)'s model for the magnetic field strength has it constant for densities below 100 m_p/cm^{-3}, but our field strength continues to decline at lower densities. At higher densities the measured field strengths fit a power law with index 0.65, slightly less than that in our simulation. However this model was intended primarily to fit the data from limited measurements, whereas we have information on magnetic field strengths for every single piece of gas in our galaxy.

4.6 Comparison to Previous Work

There are some important differences between our work and previous simulations done by others. Several other groups have simulated galaxies with MHD; however, they all used lower resolutions than our simulations. As a result of this this they were able to evolve their galaxies for longer periods of time.

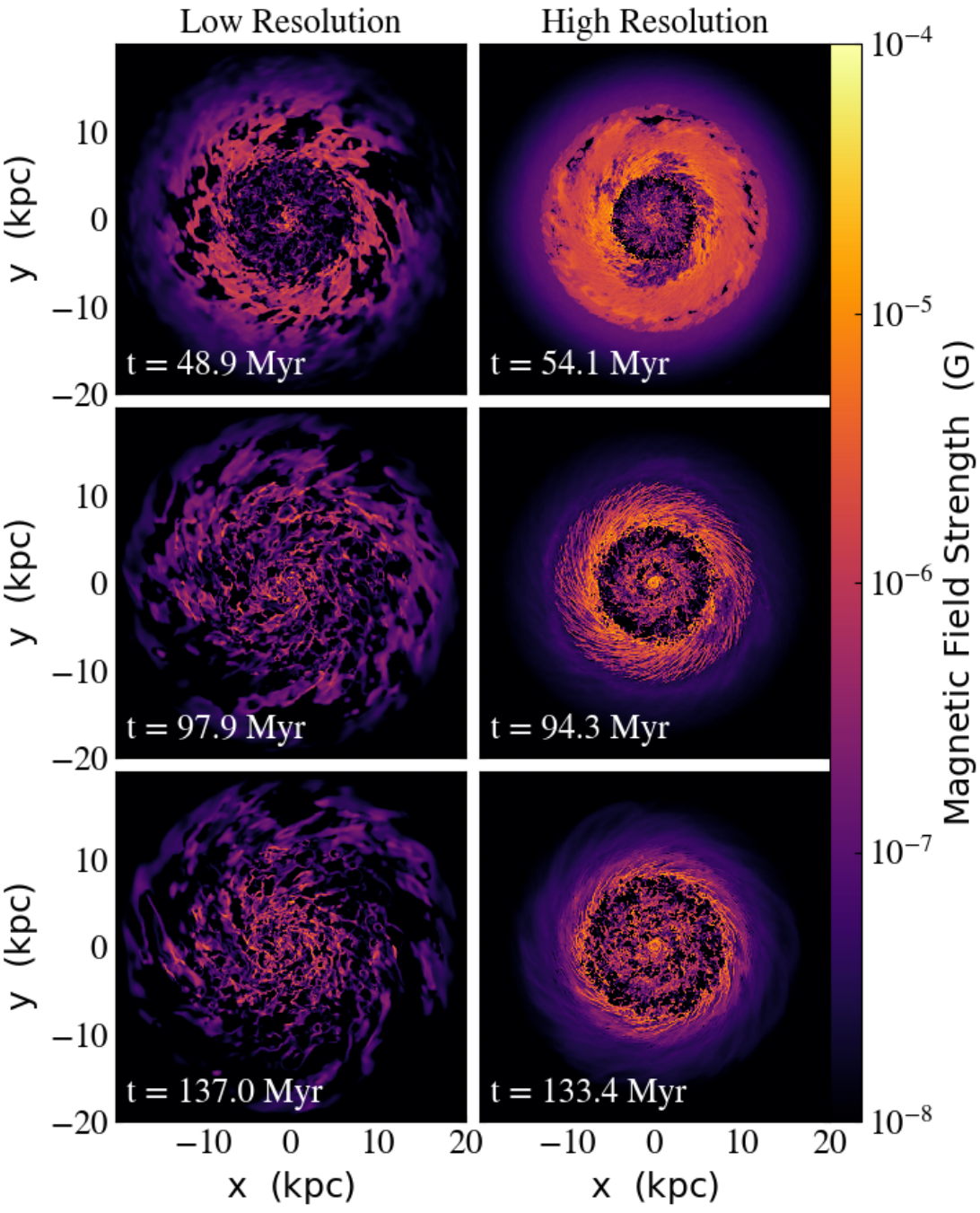

FIGURE 4.19: Time evolution of the magnetic field in each MHD galaxy. Each panel shows a slice of the magnetic field strength in the midplane.

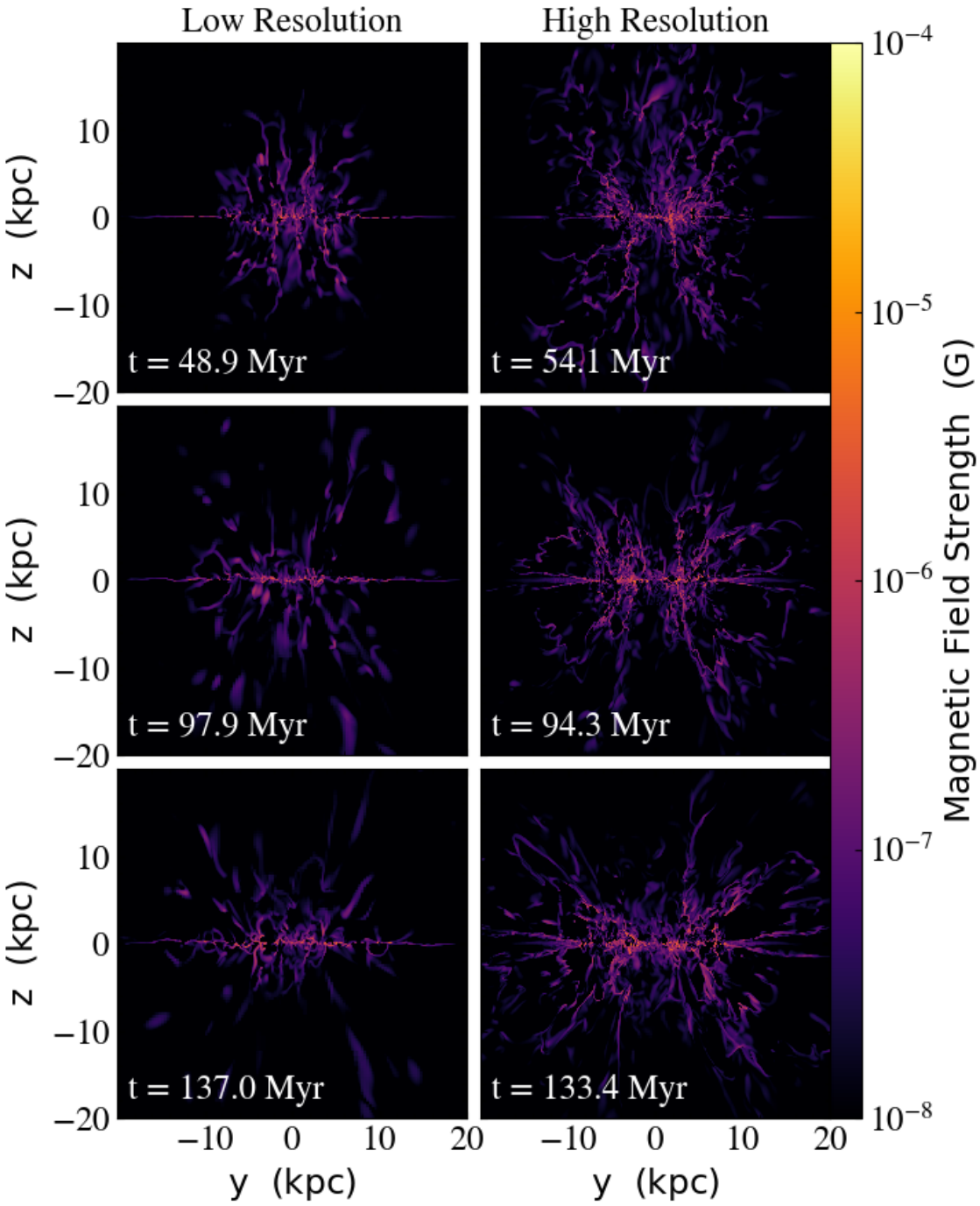

FIGURE 4.20: Time evolution of the magnetic field in each MHD galaxy. Each panel shows a slice of the magnetic field strength in the y-z plane.

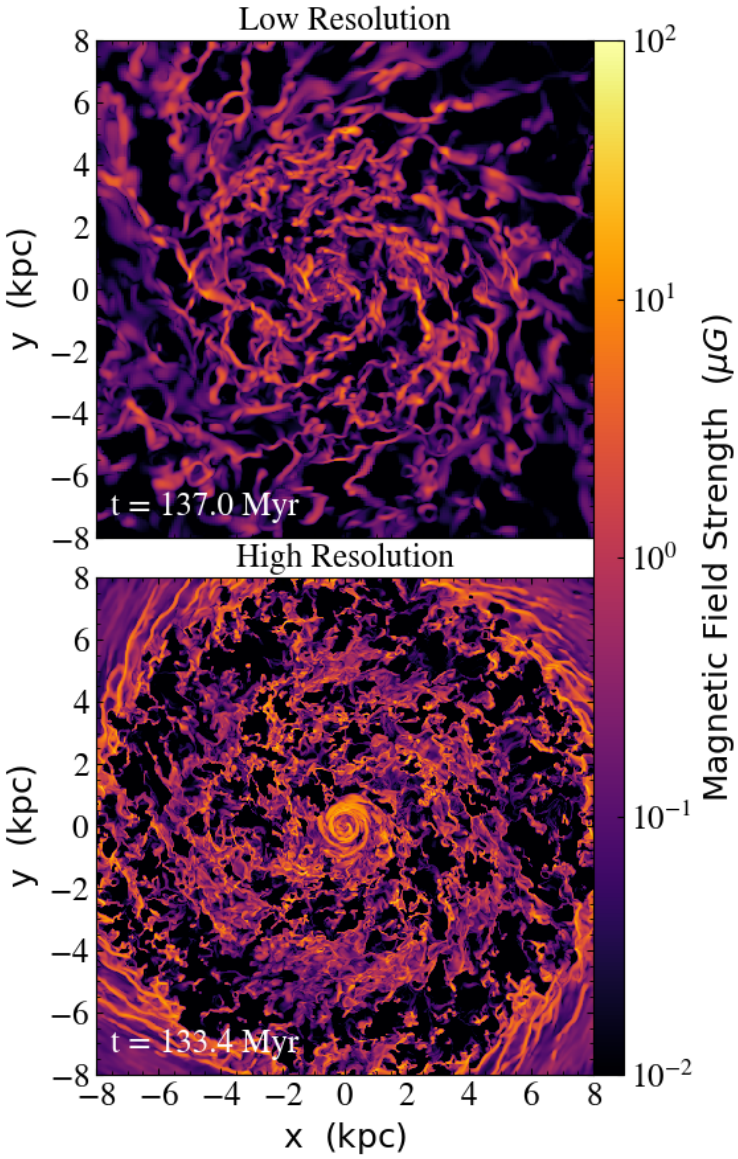

FIGURE 4.21: Central 8 kpc of each MHD galaxy in the final snapshot. Each panel shows a slice of the magnetic field strength in the x-y plane.

Körtgen et al. (2019) simulated magnetized disk galaxies and found that magnetic fields resulted in gas being pulled hundreds of parsecs above the midplane via the Parker instability without the use of stellar feedback, and also accelerated the formation of massive GMCs in the ISM. Our work has stellar feedback, so any of these massive GMCs are destroyed before they get those sizes, and we have lots of magnetic fields many kpc above the disk that are dragged out in outflows. In our work, it is unclear whether or not the Parker instability is active, or if the vertical motions in the gas are fueled primarily by feedback. Additionally our simulation does not have much gas above densities of 10^3 m_p/cm^{-3} because it is quickly converted into stars. In their work there is no active star formation but gas reaches densities of up to 10^5 m_p/cm^{-3} They also use a static gravitational potential for the stellar disk and dark matter halo, where ours is made of active particles, which could affect the development of spiral arm features and fragmentation. The magnetic fields in Körtgen et al. (2019) started with an initial scaling of B $\propto \rho^{1/2}$, but it evolved to B $\propto \rho^{2/3}$ and slightly higher in diffuse gas. Ours started as B $\propto \rho^{2/3}$ but slightly increased, as see in Figure 4.22 of Figure B1 of Körtgen et al. (2019). The increase in field strength in both simulations suggests an amplification by turbulent dynamo.

Rieder and Teyssier (2016) and Rieder and Teyssier (2017) simulated magnetized dwarf and Milky Way sized galaxies and they did include the effects of star formation and feedback; however they used a lower star formation efficiency $\epsilon_* = 0.01$. Their work has showed thermal pressure was in equipartition with turbulent pressure, but ours see turbulence dominate almost everywhere. Our enhanced turbulence could come from the higher resolution of our simulations. Their magnetic field strength grew exponentially with a timescale of $\tau = 170$ Myr. This growth rate seems consistent with the second phase of growth seen in our simulations; however, our growth rate in that phase does not appear to be resolution dependent where theirs changed based on the resolution. A key difference between our simulations is that their initial fields were much weaker than ours initially and grew many more orders of magnitude in strength.

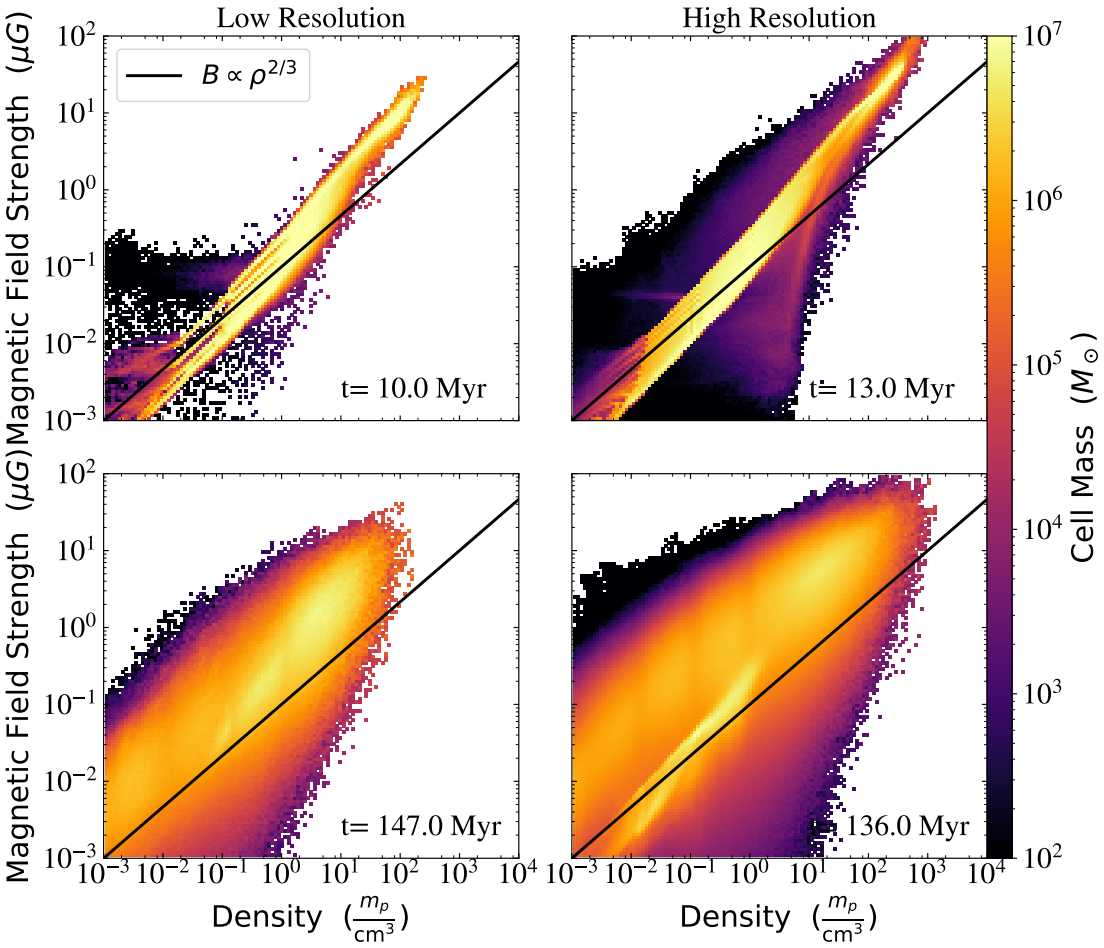

FIGURE 4.22: Two-dimensional magnetic field strength vs. density histogram for each galaxy. The colour scales with the log of the total mass in each bin. Shows an early time (top row), and a late time (bottom row). The line plotted shows a field that scales as $B \propto \rho^(2/3)$, which was the original field in the IC.

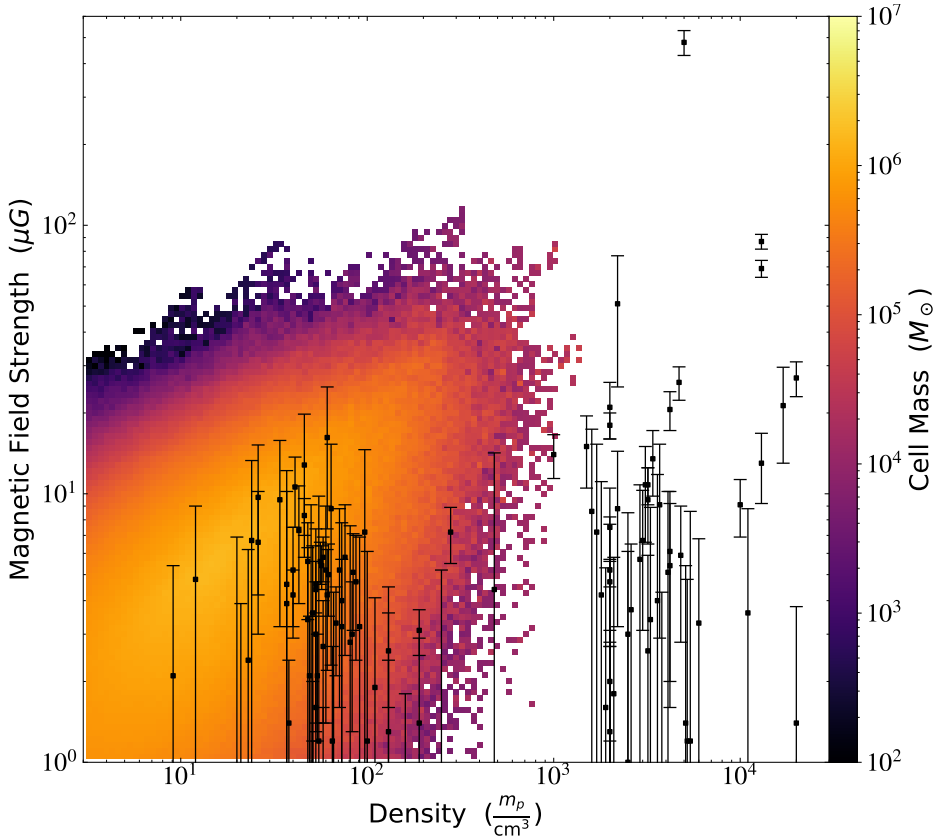

FIGURE 4.23: Two-dimensional magnetic field strength vs. density histogram for high resolution galaxy only. The colour scales with the log of the total mass in each bin. The plotted points are measured field strengths in the Milky Way from Zeeman measurements in Crutcher et al. (2010).

Chapter 5

Discussion

In this thesis we have explored the use of hydrodynamic simulations to study galaxy evolution. In Chapter 3 we conducted many different types of simulations to explore specific requirements and limitations on simulating galaxies and the ISM. We focused on the use of sub-grid models and how they interact with varying numerical resolutions. We showed that the scale height of the galaxy is a minimum size must be resolved, and confirmed results that showed periodic ISM boxes do not model outflows well. We also demonstrated the shortcoming of some simple stellar feedback models, and settled on using different models that accurately predict the heating of the ISM. We then conducted simulations of entire disk galaxies with our chosen models and showed they were able to predict the self regulating-nature of the ISM.

Once we had decided upon a set of tools, we investigated the addition of MHD into our simulations of disk galaxies in Chapter 4. MHD showed significant resolution dependence. At low resolutions, MHD played very little if any role in the evolution of the galaxy, but when increased to high resolutions it began to affect the behaviours of the gas. Most notably it led to a decreased star formation rate, more warm gas and an increased scale height. The increased scale height is particularly interesting given the decreased star formation rate, meaning the MHD galaxy had an effectively higher pressure, despite having less support from feedback. This is largely due to an enhancement in the turbulence of the gas; magnetic fields coupled kinetic energy of feedback to the gas by dragging extra gas along with them. These results confirm magnetic fields can play an important role in shaping the ISM, especially when combined with the effects of feedback.

The time evolution of the magnetic field also showed to be somewhat resolution dependent. At higher resolutions the field quickly grew to higher strengths, however it then entered a second phase of growth where the growth rates seemed to be resolution independent. The measured magnetic field strengths at the end of the simulation were consistent with magnetic field strengths measured within the Milky Way for gas of a given density, but it is unclear if they will continue to at higher densities, this is something we hope to explore in future work.

5.1 Future Work

One of the first projects we plan to continue is the running of our high resolution galaxies. Due to time constraints they were only able to evolve for 130 Myr, and they may have still been in a somewhat transient phase of their evolution. As our simulations continue to run, we will explore the long term evolution of the galaxies and determine if they settle into a steady state. We will also see if the magnetic field strengths in the high resolution galaxies saturate at the same level as the low resolution ones, like in results from Rieder and Teyssier (2017).

Another direction we would like to go is to even higher resolutions. Firstly to check for numerical convergence; Our simulations have shown that increasing the resolution changes the effects of MHD, but they may change more dramatically at even higher resolutions. It is not yet clear what the ideal resolutions are to minimize computer time while having converged results. Increasing the resolutions will additionally allow us to investigate what role magnetic fields play within GMCs, inside of a realistic galaxy environment as compared to simulations of periodic boxes which can reach high resolutions but have unrealistic behaviours. With a minimum grid size of 9 pc we still do not resolve individual GMCs or the turbulent motions and magnetic fields within them that well. To do this we plan to develop methods to do a zoom-in simulation within our isolated galaxy. We plan to increase the resolution of a small subsection of the ISM so that the lives of individual GMCs within it can be resolved and tracked.

Higher resolutions will also allow us to reach higher densities of gas, which will be necessary in comparing to measurements of magnetic field strengths; we currently barely overlap with the regions measured by observations, and while the strengths

agree well, having more overlapping data will let us confirm if we match the trends over varying densities.

Our results may also have changed if we used a different feedback method. The delayed cooling model was able to effectively heat the ISM and regulate star formation, but it did so by incorporating new free parameters such as the timescale to disable cooling. The superbubble model (Keller et al. 2014) is currently in development to use in Ramses and combining it will lead to a more realistically regulated ISM.

Finally we plan to study MHD galaxies in other environments. All of our MHD galaxies were isolated, but magnetic fields could play an important role in cluster environments. We plan to simulate galaxies moving through the magnetic fields of a cluster to determine how the external fields interact with the galaxy. One possibility is that the galaxy picks up fields from the cluster gas as it travels through them providing the galaxy with a "magnetic shielding". Our simulations are perfectly equipped to handle questions like these.

Bibliography

Adebahr, B., Krause, M., Klein, U., Heald, G., and Dettmar, R. .-.-J. (Dec. 2017). M 82 - A radio continuum and polarisation study. II. Polarisation and rotation measures. *Astronomy and Astrophysics* 608 A29, A29.

Agertz, O. and Kravtsov, A. V. (June 2016). The Impact of Stellar Feedback on the Structure, Size, and Morphology of Galaxies in Milky-Way-sized Dark Matter Halos. *Astrophysical Journal* 824(2) 79, 79.

Agertz, O., Moore, B., Stadel, J., Potter, D., Miniati, F., Read, J., Mayer, L., Gawryszczak, A., Kravtsov, A., Nordlund, Å., Pearce, F., Quilis, V., Rudd, D., Springel, V., Stone, J., Tasker, E., Teyssier, R., Wadsley, J., and Walder, R. (Sept. 2007). Fundamental differences between SPH and grid methods. *Monthly Notices of the Royal Astronomical Society* 380(3), 963–978.

Agertz, O., Teyssier, R., and Moore, B. (Jan. 2011). The formation of disc galaxies in a ΛCDM universe. *Monthly Notices of the Royal Astronomical Society* 410(2), 1391–1408.

Barnes, J. and Hut, P. (Dec. 1986). A hierarchical O(N log N) force-calculation algorithm. *Nature* 324(6096), 446–449.

Bec, J. and Khanin, K. (Aug. 2007). Burgers turbulence. 447(1-2), 1–66.

Beck, A. M., Lesch, H., Dolag, K., Kotarba, H., Geng, A., and Stasyszyn, F. A. (May 2012). Origin of strong magnetic fields in Milky Way-like galactic haloes. *Monthly Notices of the Royal Astronomical Society* 422(3), 2152–2163.

Beck, R., Brandenburg, A., Moss, D., Shukurov, A., and Sokoloff, D. (Jan. 1996). Galactic Magnetism: Recent Developments and Perspectives. *Annual Review of Astron and Astrophys* 34, 155–206.

Beck, R. and Wielebinski, R. (2013). Magnetic Fields in Galaxies. In: *Planets, Stars and Stellar Systems Vol. 5, by Oswalt, Terry D.; Gilmore, Gerard, ISBN 978-94-007-5611-3. Springer Science+Business Media Dordrecht, 2013, p. 641.* Ed. by T. D. Oswalt and G. Gilmore. Vol. 5, 641.

Benincasa, S. M., Wadsley, J., Couchman, H. M. P., and Keller, B. W. (Nov. 2016). The anatomy of a star-forming galaxy: pressure-driven regulation of star formation in simulated galaxies. *Monthly Notices of the Royal Astronomical Society* 462(3), 3053–3068.

Bigiel, F., Leroy, A., Walter, F., Brinks, E., de Blok, W. J. G., Madore, B., and Thornley, M. D. (Dec. 2008). The Star Formation Law in Nearby Galaxies on Sub-Kpc Scales. *Astronomical Journal* 136(6), 2846–2871.

Blanton, M. R. and Moustakas, J. (Sept. 2009). Physical Properties and Environments of Nearby Galaxies. *Annual Review of Astron and Astrophys* 47(1), 159–210.

Bowen, D. V., Jenkins, E. B., Tripp, T. M., Sembach, K. R., Savage, B. D., Moos, H. W., Oegerle, W. R., Friedman, S. D., Gry, C., Kruk, J. W., Murphy, E., Sankrit, R., Shull, J. M., Sonneborn, G., and York, D. G. (May 2008). The Far Ultraviolet Spectroscopic Explorer Survey of O VI Absorption in the Disk of the Milky Way. *Astrophysical Journal, Supplement* 176(1), 59–163.

Bryan, G. L., Norman, M. L., O'Shea, B. W., Abel, T., Wise, J. H., Turk, M. J., Reynolds, D. R., Collins, D. C., Wang, P., Skillman, S. W., Smith, B., Harkness, R. P., Bordner, J., Kim, J.-h., Kuhlen, M., Xu, H., Goldbaum, N., Hummels, C., Kritsuk, A. G., Tasker, E., Skory, S., Simpson, C. M., Hahn, O., Oishi, J. S., So, G. C., Zhao, F., Cen, R., Li, Y., and Enzo Collaboration (Apr. 2014). ENZO: An Adaptive Mesh Refinement Code for Astrophysics. *Astrophysical Journal, Supplement* 211(2) 19, 19.

Burstein, P., Borken, R. J., Kraushaar, W. L., and Sand ers, W. T. (Apr. 1977). Three-band observations of the soft X-ray background and some implications of thermal emission models. *Astrophysical Journal* 213, 405–407.

Carroll, B. W. and Ostlie, D. A. (2006). *An introduction to modern astrophysics and cosmology.*

Chabrier, G. (July 2003). Galactic Stellar and Substellar Initial Mass Function. *Publications of the ASP* 115(809), 763–795.

Couchman, H. M. P. (Feb. 1991). Mesh-refined P 3M: A Fast Adaptive N-Body Algorithm. *Astrophysical Journal, Letters* 368, L23.

Couchman, H. M. P., Thomas, P. A., and Pearce, F. R. (Oct. 1995). Hydra: an Adaptive-Mesh Implementation of P 3M-SPH. *Astrophysical Journal* 452, 797.

Crutcher, R. M., Wandelt, B., Heiles, C., Falgarone, E., and Troland, T. H. (Dec. 2010). Magnetic Fields in Interstellar Clouds from Zeeman Observations: Inference of Total Field Strengths by Bayesian Analysis. *Astrophysical Journal* 725(1), 466–479.

Davis Leverett, J. and Greenstein, J. L. (Sept. 1951). The Polarization of Starlight by Aligned Dust Grains. *Astrophysical Journal* 114, 206.

Dobbs, C. L., Price, D. J., Pettitt, A. R., Bate, M. R., and Tricco, T. S. (Oct. 2016). Magnetic field evolution and reversals in spiral galaxies. *Monthly Notices of the Royal Astronomical Society* 461(4), 4482–4495.

Durrer, R. and Neronov, A. (June 2013). Cosmological magnetic fields: their generation, evolution and observation. *The Astronomy and Astrophysics Review* 21 62, 62.

Ferland, G. J., Porter, R. L., van Hoof, P. A. M., Williams, R. J. R., Abel, N. P., Lykins, M. L., Shaw, G., Henney, W. J., and Stancil, P. C. (Apr. 2013). The 2013 Release of Cloudy. *Revista Mexicana de Astronomía y Astrofísica* 49, 137–163.

Field, G. B., Goldsmith, D. W., and Habing, H. J. (Mar. 1969). Cosmic-Ray Heating of the Interstellar Gas. *Astrophysical Journal, Letters* 155, L149.

Fletcher, A. (Dec. 2010). Magnetic Fields in Nearby Galaxies. In: *The Dynamic Interstellar Medium: A Celebration of the Canadian Galactic Plane Survey*. Ed. by R. Kothes, T. L. Landecker, and A. G. Willis. Vol. 438. Astronomical Society of the Pacific Conference Series, 197.

Fryxell, B., Olson, K., Ricker, P., Timmes, F. X., Zingale, M., Lamb, D. Q., MacNeice, P., Rosner, R., Truran, J. W., and Tufo, H. (Nov. 2000). FLASH: An Adaptive Mesh Hydrodynamics Code for Modeling Astrophysical Thermonuclear Flashes. *Astrophysical Journal, Supplement* 131(1), 273–334.

Fung, A. K. S. (Feb. 2012). Numerical Simulation of Self-Gravitating Gas in Astrophysical Disks using Linearized Keplerian Dynamics. MA thesis. Seattle, WA: University of Washington.

Godunov, S. K. (1959). A difference method for numerical calculation of discontinuous solutions of the equations of hydrodynamics. *Mat. Sb. (N.S.)* 47(89), 271–306.

Goldsmith, P. F., Heyer, M., Narayanan, G., Snell, R., Li, D., and Brunt, C. (June 2008). Large-Scale Structure of the Molecular Gas in Taurus Revealed by High Linear Dynamic Range Spectral Line Mapping. *Astrophysical Journal* 680(1), 428–445.

Grand, R. J. J., Gómez, F. A., Marinacci, F., Pakmor, R., Springel, V., Campbell, D. J. R., Frenk, C. S., Jenkins, A., and White, S. D. M. (May 2017). The Auriga Project: the properties and formation mechanisms of disc galaxies across cosmic time. *Monthly Notices of the Royal Astronomical Society* 467(1), 179–207.

Grisdale, K., Agertz, O., Romeo, A. B., Renaud, F., and Read, J. I. (Apr. 2017). The impact of stellar feedback on the density and velocity structure of the interstellar medium. *Monthly Notices of the Royal Astronomical Society* 466(1), 1093–1110.

Grond, J. J., Woods, R. M., Wadsley, J. W., and Couchman, H. M. P. (May 2019). TREVR: A general N $\log^2$N radiative transfer algorithm. *Monthly Notices of the Royal Astronomical Society* 485(3), 3681–3695.

Han, J. L., Manchester, R. N., van Straten, W., and Demorest, P. (Jan. 2018). Pulsar Rotation Measures and Large-scale Magnetic Field Reversals in the Galactic Disk. *Astrophysical Journal, Supplement* 234(1) 11, 11.

Heiles, C. and Crutcher, R. (2005). Magnetic Fields in Diffuse HI and Molecular Clouds. In: *Cosmic Magnetic Fields*. Ed. by R. Wielebinski and R. Beck. Vol. 664, 137.

Hernquist, L. (June 1990). An Analytical Model for Spherical Galaxies and Bulges. *Astrophysical Journal* 356, 359.

Hoang, T. and Lazarian, A. (Feb. 2014). Grain alignment by radiative torques in special conditions and implications. *Monthly Notices of the Royal Astronomical Society* 438(1), 680–703.

Hopkins, P. F. (June 2015). A new class of accurate, mesh-free hydrodynamic simulation methods. *Monthly Notices of the Royal Astronomical Society* 450(1), 53–110.

Hopkins, P. F., Kereš, D., Oñorbe, J., Faucher-Giguère, C.-A., Quataert, E., Murray, N., and Bullock, J. S. (Nov. 2014). Galaxies on FIRE (Feedback In Realistic Environments): stellar feedback explains cosmologically inefficient star formation. *Monthly Notices of the Royal Astronomical Society* 445(1), 581–603.

Hopkins, P. F., Wetzel, A., Kereš, D., Faucher-Giguère, C.-A., Quataert, E., Boylan-Kolchin, M., Murray, N., Hayward, C. C., Garrison-Kimmel, S., Hummels, C.,

Feldmann, R., Torrey, P., Ma, X., Anglés-Alcázar, D., Su, K.-Y., Orr, M., Schmitz, D., Escala, I., Sanderson, R., Grudić, M. Y., Hafen, Z., Kim, J.-H., Fitts, A., Bullock, J. S., Wheeler, C., Chan, T. K., Elbert, O. D., and Narayanan, D. (Oct. 2018). FIRE-2 simulations: physics versus numerics in galaxy formation. *Monthly Notices of the Royal Astronomical Society* 480(1), 800–863.

Jenkins, E. B. and Meloy, D. A. (Nov. 1974). A Survey with Copernicus of Interstellar O VI Absorption. *Astrophysical Journal, Letters* 193, L121.

Keller, B. W., Wadsley, J. W., Wang, L., and Kruijssen, J. M. D. (Jan. 2019). Chaos and variance in galaxy formation. *Monthly Notices of the Royal Astronomical Society* 482(2), 2244–2261.

Keller, B. W., Wadsley, J., Benincasa, S. M., and Couchman, H. M. P. (Aug. 2014). A superbubble feedback model for galaxy simulations. *Monthly Notices of the Royal Astronomical Society* 442(4), 3013–3025.

Keller, B. W., Wadsley, J., and Couchman, H. M. P. (Dec. 2016). Cosmological galaxy evolution with superbubble feedback - II. The limits of supernovae. *Monthly Notices of the Royal Astronomical Society* 463(2), 1431–1445.

Kennicutt Robert C., J. (May 1998). The Global Schmidt Law in Star-forming Galaxies. *Astrophysical Journal* 498(2), 541–552.

Kennicutt Robert C., J., Calzetti, D., Walter, F., Helou, G., Hollenbach, D. J., Armus, L., Bendo, G., Dale, D. A., Draine, B. T., Engelbracht, C. W., Gordon, K. D., Prescott, M. K. M., Regan, M. W., Thornley, M. D., Bot, C., Brinks, E., de Blok, E., de Mello, D., Meyer, M., Moustakas, J., Murphy, E. J., Sheth, K., and Smith, J. D. T. (Dec. 2007). Star Formation in NGC 5194 (M51a). II. The Spatially Resolved Star Formation Law. *Astrophysical Journal* 671(1), 333–348.

Kennicutt, R. C. and Evans, N. J. (Sept. 2012). Star Formation in the Milky Way and Nearby Galaxies. *Annual Review of Astron and Astrophys* 50, 531–608.

Kim, C.-G., Kim, W.-T., and Ostriker, E. C. (Dec. 2011). Regulation of Star Formation Rates in Multiphase Galactic Disks: Numerical Tests of the Thermal/Dynamical Equilibrium Model. *Astrophysical Journal* 743(1) 25, 25.

Kim, C.-G. and Ostriker, E. C. (Sept. 2017). Three-phase Interstellar Medium in Galaxies Resolving Evolution with Star Formation and Supernova Feedback (TIGRESS): Algorithms, Fiducial Model, and Convergence. *Astrophysical Journal* 846(2) 133, 133.

Kim, J.-h., Abel, T., Agertz, O., Bryan, G. L., Ceverino, D., Christensen, C., Conroy, C., Dekel, A., Gnedin, N. Y., Goldbaum, N. J., Guedes, J., Hahn, O., Hobbs, A., Hopkins, P. F., Hummels, C. B., Iannuzzi, F., Keres, D., Klypin, A., Kravtsov, A. V., Krumholz, M. R., Kuhlen, M., Leitner, S. N., Madau, P., Mayer, L., Moody, C. E., Nagamine, K., Norman, M. L., Onorbe, J., O'Shea, B. W., Pillepich, A., Primack, J. R., Quinn, T., Read, J. I., Robertson, B. E., Rocha, M., Rudd, D. H., Shen, S., Smith, B. D., Szalay, A. S., Teyssier, R., Thompson, R., Todoroki, K., Turk, M. J., Wadsley, J. W., Wise, J. H., Zolotov, A., and AGORA Collaboration29, t. (Jan. 2014). The AGORA High-resolution Galaxy Simulations Comparison Project. *Astrophysical Journal, Supplement* 210(1) 14, 14.

Kim, J.-h., Agertz, O., Teyssier, R., Butler, M. J., Ceverino, D., Choi, J.-H., Feldmann, R., Keller, B. W., Lupi, A., Quinn, T., Revaz, Y., Wallace, S., Gnedin, N. Y., Leitner, S. N., Shen, S., Smith, B. D., Thompson, R., Turk, M. J., Abel, T., Arraki, K. S., Benincasa, S. M., Chakrabarti, S., DeGraf, C., Dekel, A., Goldbaum, N. J., Hopkins, P. F., Hummels, C. B., Klypin, A., Li, H., Madau, P., Mandelker, N., Mayer, L., Nagamine, K., Nickerson, S., O'Shea, B. W., Primack, J. R., Roca-Fàbrega, S., Semenov, V., Shimizu, I., Simpson, C. M., Todoroki, K., Wadsley, J. W., Wise, J. H., and AGORA Collaboration (Dec. 2016). The AGORA High-resolution Galaxy Simulations Comparison Project. II. Isolated Disk Test. *Astrophysical Journal* 833(2) 202, 202.

Klein, U., Weiland, H., and Brinks, E. (June 1991). A radio-optical study of blue compact dwarf galaxies. I. Radio continuum observations. *Astronomy and Astrophysics* 246, 323–340.

Kolmogorov, A. (Jan. 1941). The Local Structure of Turbulence in Incompressible Viscous Fluid for Very Large Reynolds' Numbers. *Akademiia Nauk SSSR Doklady* 30, 301–305.

Körtgen, B., Banerjee, R., Pudritz, R. E., and Schmidt, W. (Nov. 2019). Global dynamics of the interstellar medium in magnetized disc galaxies. *Monthly Notices of the Royal Astronomical Society* 489(4), 5004–5021.

Kruijssen, J. M. D., Schruba, A., Hygate, A. e. P. S., Hu, C.-Y., Haydon, D. T., and Longmore, S. N. (Sept. 2018). An uncertainty principle for star formation - II. A new method for characterizing the cloud-scale physics of star formation and

feedback across cosmic history. *Monthly Notices of the Royal Astronomical Society* 479(2), 1866–1952.

Krumholz, M. R., Bate, M. R., Arce, H. G., Dale, J. E., Gutermuth, R., Klein, R. I., Li, Z. .-.-Y., Nakamura, F., and Zhang, Q. (Jan. 2014). Star Cluster Formation and Feedback. In: *Protostars and Planets VI*. Ed. by H. Beuther, R. S. Klessen, C. P. Dullemond, and T. Henning, 243.

Krumholz, M. R. and Federrath, C. (Feb. 2019). The Role of Magnetic Fields in Setting the Star Formation Rate and the Initial Mass Function. *Frontiers in Astronomy and Space Sciences* 6 7, 7.

Krumholz, M. R. and Tan, J. C. (Jan. 2007). Slow Star Formation in Dense Gas: Evidence and Implications. *Astrophysical Journal* 654(1), 304–315.

Lacki, B. C. and Beck, R. (Apr. 2013). The equipartition magnetic field formula in starburst galaxies: accounting for pionic secondaries and strong energy losses. *Monthly Notices of the Royal Astronomical Society* 430(4), 3171–3186.

Larson, R. B. (Mar. 1981). Turbulence and star formation in molecular clouds. *Monthly Notices of the Royal Astronomical Society* 194, 809–826.

Lemaster, M. N. and Stone, J. M. (Feb. 2009). Dissipation and Heating in Supersonic Hydrodynamic and MHD Turbulence. *Astrophysical Journal* 691(2), 1092–1108.

Leroy, A. K., Walter, F., Sandstrom, K., Schruba, A., Munoz-Mateos, J.-C., Bigiel, F., Bolatto, A., Brinks, E., de Blok, W. J. G., Meidt, S., Rix, H.-W., Rosolowsky, E., Schinnerer, E., Schuster, K.-F., and Usero, A. (Aug. 2013). Molecular Gas and Star Formation in nearby Disk Galaxies. *Astronomical Journal* 146(2) 19, 19.

Levy, R. C., Bolatto, A. D., Teuben, P., Sánchez, S. F., Barrera-Ballesteros, J. K., Blitz, L., Colombo, D., Garcıa-Benito, R., Herrera-Camus, R., Husemann, B., Kalinova, V., Lan, T., Leung, G. Y. C., Mast, D., Utomo, D., van de Ven, G., Vogel, S. N., and Wong, T. (June 2018). The EDGE-CALIFA Survey: Molecular and Ionized Gas Kinematics in Nearby Galaxies. *Astrophysical Journal* 860(2) 92, 92.

Li, M., Bryan, G. L., and Ostriker, J. P. (June 2017). Quantifying Supernovae-driven Multiphase Galactic Outflows. *Astrophysical Journal* 841(2) 101, 101.

Machida, M., Nakamura, K. E., Kudoh, T., Akahori, T., Sofue, Y., and Matsumoto, R. (Feb. 2013). Dynamo Activities Driven by Magnetorotational Instability and the Parker Instability in Galactic Gaseous Disks. *Astrophysical Journal* 764(1) 81, 81.

Martizzi, D., Fielding, D., Faucher-Giguère, C.-A., and Quataert, E. (July 2016a). Supernova feedback in a local vertically stratified medium: interstellar turbulence and galactic winds. *Monthly Notices of the Royal Astronomical Society* 459(3), 2311–2326.

Martizzi, D., Fielding, D., Faucher-Giguère, C.-A., and Quataert, E. (July 2016b). Supernova feedback in a local vertically stratified medium: interstellar turbulence and galactic winds. *Monthly Notices of the Royal Astronomical Society* 459(3), 2311–2326.

McBride, J. and Heiles, C. (Jan. 2013). An Arecibo Survey for Zeeman Splitting in OH Megamaser Galaxies. *Astrophysical Journal* 763(1) 8, 8.

McKee, C. F. and Ostriker, J. P. (Nov. 1977). A theory of the interstellar medium: three components regulated by supernova explosions in an inhomogeneous substrate. *Astrophysical Journal* 218, 148–169.

McNally, C. P., Wadsley, J., and Couchman, H. M. P. (June 2009). Self-Gravity and Angular Momentum Transport in Extended Galactic Disks. *Astrophysical Journal, Letters* 697(2), L162–L166.

Miyoshi, T. and Kusano, K. (Dec. 2005). An MHD Simulation of the Magnetosphere Based on the HLLD Approximate Riemann Solver. In: *AGU Fall Meeting Abstracts*. Vol. 2005, SM51B–1295.

Naab, T. and Ostriker, J. P. (Aug. 2017). Theoretical Challenges in Galaxy Formation. *Annual Review of Astron and Astrophys* 55(1), 59–109.

Navarro, J. F., Frenk, C. S., and White, S. D. M. (Dec. 1997). A Universal Density Profile from Hierarchical Clustering. *Astrophysical Journal* 490(2), 493–508.

Ostriker, E. C. and Shetty, R. (Apr. 2011). Maximally Star-forming Galactic Disks. I. Starburst Regulation Via Feedback-driven Turbulence. *Astrophysical Journal* 731(1) 41, 41.

Planck Collaboration et al. (Sept. 2016). Planck 2015 results. XXV. Diffuse low-frequency Galactic foregrounds. *Astronomy and Astrophysics* 594 A25, A25.

Planck Collaboration et al. (July 2018). Planck 2018 results. I. Overview and the cosmological legacy of Planck. *arXiv e-prints* arXiv:1807.06205, arXiv:1807.06205.

Price, D. J., Wurster, J., Tricco, T. S., Nixon, C., Toupin, S., Pettitt, A., Chan, C., Mentiplay, D., Laibe, G., Glover, S., Dobbs, C., Nealon, R., Liptai, D., Worpel, H., Bonnerot, C., Dipierro, G., Ballabio, G., Ragusa, E., Federrath, C., Iaconi, R.,

Reichardt, T., Forgan, D., Hutchison, M., Constantino, T., Ayliffe, B., Hirsh, K., and Lodato, G. (Sept. 2018). Phantom: A Smoothed Particle Hydrodynamics and Magnetohydrodynamics Code for Astrophysics. 35 e031, e031.

Rieder, M. and Teyssier, R. (Apr. 2016). A small-scale dynamo in feedback-dominated galaxies as the origin of cosmic magnetic fields - I. The kinematic phase. *Monthly Notices of the Royal Astronomical Society* 457(2), 1722–1738.

Rieder, M. and Teyssier, R. (Nov. 2017). A small-scale dynamo in feedback-dominated galaxies - II. The saturation phase and the final magnetic configuration. *Monthly Notices of the Royal Astronomical Society* 471(3), 2674–2686.

Robertson, B. E. and Kravtsov, A. V. (June 2008). Molecular Hydrogen and Global Star Formation Relations in Galaxies. *Astrophysical Journal* 680(2), 1083–1111.

Ruzmaikin, A. A., Sokolov, D. D., and Shukurov, A. M. (1988). *Magnetic Fields of Galaxies*. Vol. 133.

Saintonge, A., Catinella, B., Tacconi, L. J., Kauffmann, G., Genzel, R., Cortese, L., Davé, R., Fletcher, T. J., Graciá-Carpio, J., Kramer, C., Heckman, T. M., Janowiecki, S., Lutz, K., Rosario, D., Schiminovich, D., Schuster, K., Wang, J., Wuyts, S., Borthakur, S., Lamperti, I., and Roberts-Borsani, G. W. (Dec. 2017). xCOLD GASS: The Complete IRAM 30 m Legacy Survey of Molecular Gas for Galaxy Evolution Studies. *Astrophysical Journal, Supplement* 233(2) 22, 22.

Scannapieco, C., Wadepuhl, M., Parry, O. H., Navarro, J. F., Jenkins, A., Springel, V., Teyssier, R., Carlson, E., Couchman, H. M. P., Crain, R. A., Dalla Vecchia, C., Frenk, C. S., Kobayashi, C., Monaco, P., Murante, G., Okamoto, T., Quinn, T., Schaye, J., Stinson, G. S., Theuns, T., Wadsley, J., White, S. D. M., and Woods, R. (June 2012). The Aquila comparison project: the effects of feedback and numerical methods on simulations of galaxy formation. *Monthly Notices of the Royal Astronomical Society* 423(2), 1726–1749.

Schawinski, K., Urry, C. M., Simmons, B. D., Fortson, L., Kaviraj, S., Keel, W. C., Lintott, C. J., Masters, K. L., Nichol, R. C., Sarzi, M., Skibba, R., Treister, E., Willett, K. W., Wong, O. I., and Yi, S. K. (May 2014). The green valley is a red herring: Galaxy Zoo reveals two evolutionary pathways towards quenching of star formation in early- and late-type galaxies. *Monthly Notices of the Royal Astronomical Society* 440(1), 889–907.

Schaye, J., Crain, R. A., Bower, R. G., Furlong, M., Schaller, M., Theuns, T., Dalla Vecchia, C., Frenk, C. S., McCarthy, I. G., Helly, J. C., Jenkins, A., Rosas-Guevara, Y. M., White, S. D. M., Baes, M., Booth, C. M., Camps, P., Navarro, J. F., Qu, Y., Rahmati, A., Sawala, T., Thomas, P. A., and Trayford, J. (Jan. 2015). The EAGLE project: simulating the evolution and assembly of galaxies and their environments. *Monthly Notices of the Royal Astronomical Society* 446(1), 521–554.

Schmidt, M. (Mar. 1959). The Rate of Star Formation. *Astrophysical Journal* 129, 243.

Smith, B. D., Bryan, G. L., Glover, S. C. O., Goldbaum, N. J., Turk, M. J., Regan, J., Wise, J. H., Schive, H.-Y., Abel, T., Emerick, A., O'Shea, B. W., Anninos, P., Hummels, C. B., and Khochfar, S. (Dec. 2016). *Grackle: Chemistry and radiative cooling library for astrophysical simulations.*

Sparke, L. S. and Gallagher John S., I. (2007). *Galaxies in the Universe: An Introduction.*

Springel, V. (Dec. 2005). The cosmological simulation code GADGET-2. *Monthly Notices of the Royal Astronomical Society* 364(4), 1105–1134.

Springel, V. (Jan. 2010). E pur si muove: Galilean-invariant cosmological hydrodynamical simulations on a moving mesh. *Monthly Notices of the Royal Astronomical Society* 401(2), 791–851.

Springel, V., Pakmor, R., Pillepich, A., Weinberger, R., Nelson, D., Hernquist, L., Vogelsberger, M., Genel, S., Torrey, P., Marinacci, F., and Naiman, J. (Mar. 2018). First results from the IllustrisTNG simulations: matter and galaxy clustering. *Monthly Notices of the Royal Astronomical Society* 475(1), 676–698.

Stadel, J. G. (Jan. 2001). Cosmological N-body simulations and their analysis. PhD thesis. UNIVERSITY OF WASHINGTON.

Stinson, G., Seth, A., Katz, N., Wadsley, J., Governato, F., and Quinn, T. (Dec. 2006). Star formation and feedback in smoothed particle hydrodynamic simulations - I. Isolated galaxies. *Monthly Notices of the Royal Astronomical Society* 373(3), 1074–1090.

Stone, J. M., Gardiner, T. A., Teuben, P., Hawley, J. F., and Simon, J. B. (Sept. 2008). Athena: A New Code for Astrophysical MHD. *Astrophysical Journal, Supplement* 178(1), 137–177.

Sun, J., Leroy, A. K., Schruba, A., Rosolowsky, E., Hughes, A., Kruijssen, J. M. D., Meidt, S., Schinnerer, E., Blanc, G. A., Bigiel, F., Bolatto, A. D., Chevance, M.,

Groves, B., Herrera, C. N., Hygate, A. e. P. S., Pety, J., Querejeta, M., Usero, A., and Utomo, D. (June 2018). Cloud-scale Molecular Gas Properties in 15 Nearby Galaxies. *Astrophysical Journal* 860(2) 172, 172.

Tasker, E. J., Wadsley, J., and Pudritz, R. (Mar. 2015). Star Formation in Disk Galaxies. III. Does Stellar Feedback Result in Cloud Death? *Astrophysical Journal* 801(1) 33, 33.

Teyssier, R. (Apr. 2002). Cosmological hydrodynamics with adaptive mesh refinement. A new high resolution code called RAMSES. *Astronomy and Astrophysics* 385, 337–364.

Tielens, A. G. G. M. (2005). *The Physics and Chemistry of the Interstellar Medium.*

Toomre, A. (May 1964). On the gravitational stability of a disk of stars. *Astrophysical Journal* 139, 1217–1238.

Toomre, A. and Toomre, J. (Dec. 1972). Galactic Bridges and Tails. *Astrophysical Journal* 178, 623–666.

Toro, E. F., Spruce, M., and Speares, W. (July 1994). Restoration of the contact surface in the HLL-Riemann solver. *Shock Waves* 4(1), 25–34.

Tremmel, M., Karcher, M., Governato, F., Volonteri, M., Quinn, T. R., Pontzen, A., Anderson, L., and Bellovary, J. (Sept. 2017). The Romulus cosmological simulations: a physical approach to the formation, dynamics and accretion models of SMBHs. *Monthly Notices of the Royal Astronomical Society* 470(1), 1121–1139.

Truelove, J. K., Klein, R. I., McKee, C. F., Holliman John H., I., Howell, L. H., and Greenough, J. A. (Nov. 1997). The Jeans Condition: A New Constraint on Spatial Resolution in Simulations of Isothermal Self-gravitational Hydrodynamics. *Astrophysical Journal, Letters* 489(2), L179–L183.

Vogelsberger, M., Genel, S., Springel, V., Torrey, P., Sijacki, D., Xu, D., Snyder, G., Nelson, D., and Hernquist, L. (Oct. 2014). Introducing the Illustris Project: simulating the coevolution of dark and visible matter in the Universe. *Monthly Notices of the Royal Astronomical Society* 444(2), 1518–1547.

Wadsley, J. W., Stadel, J., and Quinn, T. (Feb. 2004). Gasoline: a flexible, parallel implementation of TreeSPH. 9(2), 137–158.

Wadsley, J. W., Keller, B. W., and Quinn, T. R. (Oct. 2017). Gasoline2: a modern smoothed particle hydrodynamics code. *Monthly Notices of the Royal Astronomical Society* 471(2), 2357–2369.

Walch, S., Girichidis, P., Naab, T., Gatto, A., Glover, S. C. O., Wünsch, R., Klessen, R. S., Clark, P. C., Peters, T., Derigs, D., and Baczynski, C. (Nov. 2015). The SILCC (SImulating the LifeCycle of molecular Clouds) project - I. Chemical evolution of the supernova-driven ISM. *Monthly Notices of the Royal Astronomical Society* 454(1), 238–268.

Walter, F., Brinks, E., de Blok, W. J. G., Bigiel, F., Kennicutt Robert C., J., Thornley, M. D., and Leroy, A. (Dec. 2008). THINGS: The H I Nearby Galaxy Survey. *Astronomical Journal* 136(6), 2563–2647.